Synchronization in complex systems with multiple time scales

Kumulative Dissertation

zur Erlangung des akademischen Grades
Doktor der Naturwissenschaften (Dr. rer. nat.)
in der Wissenschaftsdisziplin Nichtlineare Dynamik / Datenanalyse

eingereicht an der
Mathematisch-Naturwissenschaftlichen Fakultät
Universität Potsdam

von
André Bergner

Potsdam, 18. August 2011

Published online at the
Institutional Repository of the University of Potsdam:
URL http://opus.kobv.de/ubp/volltexte/2011/5340/
URN urn:nbn:de:kobv:517-opus-53407
http://nbn-resolving.de/urn:nbn:de:kobv:517-opus-53407

Abstract

In the present work synchronization phenomena in complex dynamical systems exhibiting multiple time scales have been analyzed. Multiple time scales can be active in different manners. Three different systems have been analyzed with different methods from data analysis.

The first system studied is a large heterogenous network of bursting neurons, that is a system with two predominant time scales, the fast firing of action potentials (spikes) and the burst of repetitive spikes followed by a quiescent phase. This system has been integrated numerically and analyzed with methods based on recurrence in phase space. An interesting result are the different transitions to synchrony found in the two distinct time scales. Moreover, an anomalous synchronization effect can be observed in the fast time scale, i.e. there is range of the coupling strength where desynchronization occurs.

The second system analyzed, numerically as well as experimentally, is a pair of coupled CO_2 lasers in a chaotic bursting regime. This system is interesting due to its similarity with epidemic models. We explain the bursts by different time scales generated from unstable periodic orbits embedded in the chaotic attractor and perform a synchronization analysis of these different orbits utilizing the continuous wavelet transform. We find a diverse route to synchrony of these different observed time scales.

The last system studied is a small network motif of limit cycle oscillators. Precisely, we have studied a hub motif, which serves as elementary building block for scale-free networks, a type of network found in many real world applications. These hubs are of special importance for communication and information transfer in complex networks. Here, a detailed study on the mechanism of synchronization in oscillatory networks with a broad frequency distribution has been carried out. In particular, we find a remote synchronization of nodes in the network which are not directly coupled. We also explain the responsible mechanism and its limitations and constraints. Further we derive an analytic expression for it and show that information transmission in pure phase oscillators, such as the Kuramoto type, is limited. In addition to the numerical and analytic analysis an experiment consisting of electrical circuits has been designed. The obtained results confirm the former findings.

Zusammenfassung

In der vorliegenden Arbeit wurden Synchronisationsphänomene in komplexen Systemen mit mehreren Zeitskalen untersucht. Es gibt mehrere Möglichkeiten wie diese verschiedenen Zeitskalen vorkommen können. Drei verschiedene Systeme, jedes mit einer anderen Art von zeitlicher Multiskalität, wurden mit unterschiedlichen Methoden der Datenanalyse untersucht.

Das erste untersuchte System ist ein ausgedehntes heterogenes Netzwerk von Neuronen mit zwei dominanten Zeitskalen, zum einen die schnelle Folge von Aktionspotenzialen und zum anderen einer abwechselnden Folge von einer Phase von Aktionspotenzialen und einer Ruhephase. Dieses System wurde numerisch integriert und mit Methoden der Phasenraumrekurrenz untersucht. Ein interessantes Ergebnis ist der unterschiedliche Übergang zur Synchronisation der Neuronen auf den beiden verschiedenen Zeitskalen. Des weiteren kann auf der schnellen Zeitskala eine anomale Synchronisation beobachtet werden, d.h. es gibt einen Bereich der Kopplungsstärke in dem es zu einer Desynchronisation kommt.

Als zweites wurde, sowohl numerisch als auch experimentell, ein System von gekoppelten CO_2 Lasern untersucht, welche in einem chaotischen *bursting* Modus arbeiten. Dieses System ist auch durch seine Äquivalenz zu Epidemiemodellen interessant. Wir erklären die *Bursts* durch unterschiedliche Zeitskalen, welche durch in den chaotischen Attraktor eingebettete instabile periodische Orbits generiert werden. Wir führen eine Synchronisationsanalyse mit Hilfe der kontinuierlichen Wavelettransformation durch und finden einen unterschiedlichen Übergang zur Synchronisation auf den unterschiedlichen Zeitskalen.

Das dritte analysierte System ist ein Netzwerkmotiv von Grenzzyklusoszillatoren. Genauer handelt es sich um ein Nabenmotiv, welches einen elementaren Grundbaustein von skalenfreien Netzwerken darstellt, das sind Netzwerke die eine bedeutende Rolle in vielen realen Anwendungen spielen. Diese Naben sind von besonderer Bedeutung für die Kommunikation und den Informationstransport in komplexen Netzwerken. Hierbei wurde eine detaillierte Untersuchung des Synchronisationsmechanismus in oszillatorischen Netzwerken mit einer breiten Frequenzverteilung durchgeführt. Insbesondere beobachten wir eine Fernsynchronisation von Netzerkknoten, die nur indirekt über andere Oszillatoren miteinander gekoppelt sind. Wir erklären den zu Grunde liegenden Mechanismus und zeigen dessen Grenzen und Bedingungen auf. Des weiteren leiten wir einen analytischen Ausdruck für den Mechanismus her und zeigen, dass eine Informationsübertragung in reinen Phasenoszillatoren, wie beispielsweise vom Kuramototyp, eingeschränkt ist. Diese Ergebnisse konnten wir durch Experimente mit elektrischen Schalkreisen bestätigen.

dedicated to
Helena, Dalia, and Filip

Contents

1 Introduction

Throughout history natural sciences are continuously moving from simplicity to complexity. In the past we had been focusing on simple fundamental rules governing nature, such as the harmonic ratios perceived in swinging strings studied by the Pythagoreans or the newtonian laws governing the movements of rigid bodies. The systems studied had been becoming more complex within the 19^{th} century, when the laws of thermodynamics had been discovered which later could be derived by describing matter as made up from tremendously many particles governed, again, by simple rules. This advance, and that of many other fields not given here, was driven by a rapid progress in mathematics and in the design of new experiments. However, if we limit our tools to math merely, we are only able to describe simple phenomena or complex systems close to an equilibrium state within a statistical framework.

With the advent of computers in the second half of the 20^{th} century scientists received a new instrument for studying nature, in addition to experiments and mathematics. Now, it has become possible to conduct numerical experiments by simulating equations with the help of computers and, moreover, using computers to analyze data using complex algorithms. The mathematical treatment of a problem becomes very hard or, as in most cases, undoable, as soon as the studied system becomes to complex or even chaotic. In these cases the mathematical shortcut from the describing equation to some observable of interest, say, the time to reach some threshold, is not available and one has to integrate the equations entirely.

With the help of computers scientists have made a lot of progress in understanding the sublime complexity of nature. Many applications have been developed by this approach, these are, for instance, the weather forecast, chaos theory, advances in genetics and bioinformatics, solving the Einstein field equation, and, forthcoming, the simulation of an entire human brain as it is aimed by several projects. In this present work a phenomenon from nonlinear science and theory of complexity has been studied, namely synchronization.

Synchronization is ubiquitous in nature and technology. As soon as a dynamical process possesses some rhythm, i.e. a recurring dynamical pattern within its course of time, one can speak about oscillation. If two or more rhythmic systems are interacting in some way, they might synchronize as well, that is, they adapt their rhythms to a common one [1] in order to communicate [2], or to minimize the their energy [3].

Synchronization is fundamental in biology where rhythms are found everywhere. For instance, on a molecular scale within cells genetic oscillators may synchronize and control important cellular processes [4]. On a cellular scale in particular the brain is a common example, which can be understood as a huge network of interacting oscillators [5]. On the scale of whole organs synchronization can be found in the cardiorespiratory system [6]. And on the scale of many interacting organisms one finds rhythms and synchronization

thereof in outbreaks of diseases, such as measles [7]. Synchronization is applied in medicine, where for example an pathological synchronization is spawned by Parkinson's disease and one wishes to suppress this unwanted synchronization in order to remove the symptoms [8].

Synchronization has numerous applications in engineering, e.g. in communication, where synchronization has long been used within phase locked loops [9] in FM radio transmission. Today it is studied widely in in the context of communication based on chaotic synchronization [2]. It has applications in robotics, where it is used to self-organize the coordination of robot legs [10]. Further, synchronization is very common in the huge field of control theory where suppressing or enhancing synchronization is used in many applications [11].

One particular attribute of synchronization is its ability to bring order to chaos. By synchronizing, parts of large turbulent systems self-organize and structures emerge on larger scales, while on a smaller scale chaotic or random behavior may still remain. Hence, gaining knowledge about synchronization generally helps understanding self-organization and information transmission in complex systems.

A fundamental property of complex systems is the presence of multiple scales, spatially as well as temporally. When dealing with rhythms and synchronization especially the multiple time scales are of interest. Picking up the biological example from above, multiple time scales can be found all over in biological systems. A popular and widely studied system exhibiting multiple time scales is the neuron. Here on the one hand one finds the scale of a singular action potential, usually referred to as spike, and repetitions of these, and on the other hand, there is the scale of bursts of those spikes, i.e. a fast repetition of spikes followed by a quiescent phase. In [13] we study the interaction in large networks of such bursting neurons.

While the multiple time scales found in bursting patterns of neurons are quite obvious, the multiple time scales present in epidemic models [7] are more devious, but can be revealed using wavelet transforms. In [14] we have studied synchronization of a pair of coupled CO_2 lasers and a model thereof. This model has been shown to share the same underlying topology with SEIR measles model [12]. Hence, insights we have gained within laser physics can be carried over to ecology and epidemiology.

While the former two mentioned multiple time scale patterns are an emergent property of the interactions of elementary parts of one integral unit, multiple time scales can also appear as a heterogeneity in a network of interacting units, i.e. a network of, say, oscillators each one possessing its own characteristic time scale which is (extremely) different across the network. In [15] we have studied such a situation and analyzed the synchronization properties found in such a system.

Multiple time scale systems are always challenging to model and analyze. For instance, taming the multiple scales and their extensive interdependencies observed in turbulent fluids is a huge topic in the field of fluid dynamics. Especially when heterogeneity is

introduced in systems with many time and even spatial scales, untangling and understanding the emerging effects is very complicated. This present work aims to shed some more light on synchronization effects found in multiple time scale systems.

2 Discussion

In the following I will discuss the mathematical and physical tools and concepts used in our publications [13–15]. I will start with networks, which have become a paradigmatic model for complexity. I will continue with the concept of recurrence which is fundamental in chaotic and complex systems. Next, I will give a short introduction to mathematical tools for time scale separation, in particular the wavelet transform. Finally, I present a quick overview of synchronization and discuss the implications thereof especially important within my work, while also combining with the former introduced concepts (networks, recurrence, wavelets).

2.1 Networks

Within the fields of nonlinear dynamics and complex system theory networks are used as a *skeleton* for dynamical systems [18–20]. Especially networks of oscillatory units are studied widely [21–23], since they serve as a modeling basis for a variety of systems, as for instance in neuroscience [5], in pattern recognition [24], or in engineering [10] (see [22] and [25] for a list of applications).

In the recent years complex networks have gained a lot of attraction in several areas of science and engineering. The study of networks is not new—mathematicians have been studying abstract networks within the field of graph theory, epidemiologists have been studying the spreading of diseases and epidemics, electrical engineers have been designing circuits as networks of discrete electrical components, and many more—but their unified study across many scientific disciplines is. This was in particular due to two seminal papers.

The first one by Watts and Strogatz published in *Nature* in 1998, who approached the famous small-world effect[1] with the tools of statistical physics [16] and showed that the average path length decreases drastically if a network possess sufficiently many shortcut links. The second paper was published in *Science* in 1999 by Barabási and Albert, who discovered that many natural networks obey a scaling law in their degree distribution.

Trivial networks, such as a chain or a grid of nodes, or an all-to-all coupled network, can be treated quite easily due to their high degree of symmetry. For complex networks

[1] The small-world effect had been first reported in an experimental study by S. Milgram examining the average path length in social networks [18]. This effects is also known as *six degrees of separation*.

usually no such symmetries exist and one needs to find other ways to describe and analyze their complex topology. The degree distribution $P(k)$ is one of the first properties analyzed. That is, the probability P to find a node with degree k, i.e. a node connected to exactly k other nodes. Many other measures, such as clustering coefficient, shortest path length or in-betweenness-centrality, have been introduced to characterize certain properties of networks [20].

The Scale-free networks, discovered by Barabási and Albert, are characterized by a heavy tailed degree distribution. This manifests in the network by a small set of nodes holding the bulk of all links while the major part of nodes is connected to a few other nodes only. These heavily connected nodes are called *hubs*. Often a mixture of the scale-free and the small-world property is observed, as one usually finds in particular densely connected hubs.

A hub motif is a small star like network which captures the essence of the hubs found in large networks. Network motifs have become a popular tool to study essential properties of complex networks on a small scale in addition to the statistic measures. These hubs are an integral part of many real world networks. Thus, investigating their role in a synchronization and communication framework gives interesting insights on self-organization in complex, in particular scale-free networks. In our paper [15] we study such a hub motif of limit-cycle oscillators and focus on a heterogenous distribution of the oscillators' natural frequencies. In real world systems one hardly finds a situation in which all components are identical. Instead a parameter mismatch accommodates this usually perceived imperfection. And, as we show, new phenomena can be discovered here.

2.2 Recurrence

The idea of recurrence, that is, a system returns after a certain time to a state (or a series of states) it had been visiting before, is old and was discussed already by the Pythagoreans and can be found in different forms in several cultures. It gained a lot of popularity through the books of Friedrich Nietzsche and his idea of eternal return [27]. In physics and mathematics the concept of recurrence was introduced by Henry Poincaré who proved in his letter [28], that any conservative system returns infinitely many times arbitrary closely to its initial conditions [29].

As well as many other concepts the recurrence concept could not be applied in practice without the aid of computers. In the late eighties when computer power had become strong enough, Eckmann et al. [30] introduced recurrence plots (RPs) to visualize the recurrences of dynamical systems [29]. A recurrence plot is a graphic visualization of the recurrence matrix. For a given sampled trajectory $\{\vec{x}_n\}_{n=1}^{N}$ of the system in phase

space the recurrence matrix is defined

$$R_{nm}^{(\epsilon)} = \begin{cases} 1 : \| \vec{x}_n - \vec{x}_m \| \leq \epsilon \\ 0 : \| \vec{x}_n - \vec{x}_m \| > \epsilon \end{cases}. \quad (1)$$

In the resulting matrix a "1" marks the point n in time when the system has returned into the ϵ-neighborhood of time m with respect to the norm $\| \, . \, \|$, otherwise the entry will be zero. The threshold ϵ depends on the size of the attractor in phase space. This threshold value is associated with the recurrence rate (ratio of ones and zeros in the recurrence matrix), and is in practice usually controlled by this one.

The recurrence approach has become a successful tool in nonlinear data analysis. In order for it to be applied either the full phase space has to be known or methods of phase space reconstruction need to be applied [31]. Even though many methods in nonlinear science don't relate explicitly to the idea of recurrence, it nevertheless lies at the heart of many applications. Several techniques based on recurrence have been proposed, such as recently introduced recurrence networks, where the idea of recurrence is combined with methods of network theory [32]. A detailed discussion of recurrence analysis and its applications can be found in [29].

In their paper [33] Romano et al. introduce a recurrence based measure to detect phase synchronization in coupled chaotic systems with non-phase-coherent attractors. This method is based on the return probability $P_\epsilon(\tau)$ which can be estimated from the recurrence matrix:

$$P_\epsilon(\tau) \approx \frac{\sum_{n=1}^{N-\tau} R_{n,n+\tau}^{(\epsilon)}}{N-\tau}. \quad (2)$$

The value $P_\epsilon(\tau)$ is the probability that a system returns to a former visited region in phase space after the time τ. In [13] we use this approach to analyze phase synchronization in a network of bursting neurons. A similar approach based on recurrence in phase space to detect phase synchronization has been proposed by Pereira et al. [34] which we utilized in [15] to confirm results obtained with other methods. In section 2.4 I discuss both methods in more detail in the context of synchronization and its application therein.

When analyzing systems with multiple time scales one needs to distinguish between those time scales. Recurrence analysis is not the tool to manage this. Although, by tuning the recurrence rate at least some selection of scale is possible as it is used in [13] in combination with linear filter techniques. Nevertheless, when dealing with several time scales other, more appropriate tools exist, which are discussed in the following.

2.3 Wavelets

The usual tool to access different time scales within a signal is the Fourier transform[2] which has been introduced by Fourier 1822 in the analysis of the heat equation [35]. The

[2] practically the Fourier series is used, due to the finiteness of any real signal

Fourier transform is one of the most useful tools developed in higher mathematics and is today one of the first algorithms which gets implemented when a new hardware sees the light of day, as, for instance, the recently introduced massively parallel processors used in modern graphics cards.

However, the Fourier transform lacks in one fundamental property: time resolution, because it decomposes a signal into a basis of pure harmonic functions $b(\omega) = e^{i\omega t}$, which are completely unlocalized. Thus, it is not able to give any information on the moment in time a frequency is occurring, or, in a more general sense, no information on instationarities of frequencies in the signal. In order to compute standard indices of phase synchronization, as introduced in Sec. 2.4, one needs to have access to the instantaneous phase of a signal. With the Fourier transform there is just one global phase for each frequency, which renders it useless in detecting phase synchronization.

A general solution to this problem is to localize the underlying basis functions $b(\omega)$ by multiplying them with a window function. The most straight forward approach is to use a fixed gaussian window, due to its nice mathematical properties. This approach is today known as Gabor transform, as it has been introduced by Gabor 1946 in order to reduce the bandwidth of sound when sending it through a communication channel [36, 37]. The window width is an additional parameter which can be tuned either to a better time localization or to a better frequency localization. Both, time and frequency, cannot be localized arbitrary sharp simultaneously, due to the time-frequency uncertainty (mathematical analogue to the Heisenberg uncertainty known from quantum mechanics).

The today's most popular approach for time-frequency analysis (and synthesis) is the wavelet transform, which is based on the idea to use small wavelets introduced by Morlet et al. [38] in the analysis of seismic waves in geophysics. In contrary to the Gabor transform, the wavelet transform does not keep the window fixed, but instead fixates the shape of the waveform itself, i.e. within the window the number of oscillations remains constant. This approach is more natural and accommodates the fact that the resulting transform remains invariant but a scaling factor under a rescaling in time of the analyzed signal.

The wavelet transform[3] $w(s,t)$ of a signal $x(t)$ with respect to the wavelet $\psi(t)$ is given by

$$w_\psi(s,t) \;=\; \frac{1}{s}\int_{\mathbb{R}} \psi\left(\frac{t'-t}{s}\right) x(t')\; dt', \tag{3}$$

where s is the scale, which is the inverse of the analyzed frequency, given that the wavelet has been normalized to frequency 1. The wavelet $\psi(t)$ can be an arbitrary function, which must be localized and with zero mean.[4] There are two ways to read and

[3] I use *wavelet transform* synonymously for *continuous wavelet transform*. Usually one needs to distinguish to the *discrete wavelet transform*, which is studied widely in mathematics and signal processing, but mainly not as a tool for data analysis.

[4] This is based on a rather mathematical reasoning. Discussion thereof can be found in [39] or [40].

understand equation (3), either as written now, as a scalar product, i.e. a given signal is compared with a family of dilated and translated wavelets, or, when rewritten as a convolution integral, it can be seen as a constant-Q bandpass filter bank.[5]

An interesting aspect important for synchronization analysis is, that when choosing a particular class of complex wavelet, so called progressive (or analytic) wavelets, one has immediate access to the instantaneous amplitude and phase for any point in the time-frequency plane. These kind of wavelet eliminate negative frequencies and, thus, implicitly perform a Hilbert transform. This we utilize in our paper [14] to access the instantaneous phase of the signal on every time scale.

Due to its nice mathematical properties, there has been an explosive growth in publication on the wavelet transform, its theory and applications (e.g. frame theory, filter banks, singularity detection). Moreover, there are also many other attempts to tackle the time-frequency problem, each approach having its benefits and downsides. In the following three popular approaches will be given. Firstly, the Wigner-Ville distribution, which originated in quantum theory, is, due to its nonlinear nature, able to bypass the time-frequency uncertainty and provide a perfect localization in the time-frequency plane. However, the drawback is the generation of cross-terms which are artifacts of the nonlinear transform and not true elements of the signal [41]. Nevertheless, several filter techniques exist, which try to eliminate the cross-terms, but thereby also destroying the sharp time-frequency localization. Secondly, empirical mode decompositions (also known as Hilbert-Huang transform) [42] is an algorithmic approach also able to extract perfectly localized time-frequency modes from a signal, but it lacks in a proper theory and explanation of the obtained modes. Thirdly, matching pursuit [43] is another popular method, which uses dictionaries of some kind of wavelets. Even though the problem can be formulated mathematically rigorously, it is only possible to approximate the solution, due to the method's inverse nature (NP hard to solve). Several algorithms to speed up the problem exist, though.

All the above approaches have in common that they fail for signals which are too complex or too noisy, either because of interactions between signal parts (Wigner-Ville transform, empirical mode decomposition), or due to a rapidly growing computational cost (matching pursuit). It should also be noted that a unique time-frequency transform does not exist. The choice of the method depends on the precise problem one is attempting to solve and its constraints. The wavelet approach has become that popular, as it makes the best trade off between side effects and generality, and due to its nice analytically properties.

[5] In a constant-Q filter bank the ratio of the filter's bandwidth and the filter's center frequency is constant for all filters.

2.4 Synchronization

Synchronization is a fundamental phenomenon appearing in many systems made up of interacting oscillatory nonlinear units. Synchronization can appear in limit cycle systems as well as in chaotic systems. Several types of synchronization can be distinguished, including complete, lag, generalized, and phase synchronization [1].

Complete synchronization implies the exact coincidence of the system's states, $\vec{x}_1(t) = \vec{x}_2(t)$, and is only possible for interacting identical systems. In the case of a small parameter mismatch, however, close approximation is possible: $\vec{x}_1(t) \approx \vec{x}_2(t)$.

Generalized synchronization is defined by a functional relationship between two trajectories, $\vec{x}_2(t) = \vec{F}[\vec{x}_1(t)]$, which implies that the state $\vec{x}_2(t)$ of one system can be predicted given the state $\vec{x}_1(t)$ of the other and the functional relationship $\vec{F}(.)$ [44]. Complete synchronization can be seen as a special case of generalized synchronization with $\vec{F} = \mathbb{1}$. Generalized synchronization is accompanied by a collapse of the attractor of the coupled system from the full phase space onto a sub-manifold, the so called synchronization-manifold.

Lag synchronization is a situation in which two systems nearly coincide but shifted in time: $\vec{x}_1(t) \approx \vec{x}_2(t - \tau)$, where τ is the lag. This type can be found for intermediate coupling strengths between phase synchronization (discussed below) and complete synchronization [45].

The most general form is phase synchronization, which is also closest related to the greek term *synchronization* itself, which means "together in time". Phase synchronization is described by an adaption of the characteristic time scales of two systems. More precisely, its defined by the phase differences between the two systems being bounded, i.e. given the phases $\varphi_1(t)$ and $\varphi_2(t)$ and the finite real number θ, the following must be fulfilled:

$$|\varphi_2(t) - \varphi_1(t)| \leq \theta. \tag{4}$$

An index oftenly used for measuring the phase coherence of oscillators is the Kuramoto order parameter [46, 47] given by

$$r \;=\; \left|\langle e^{i[\varphi_n(t)-\varphi_m(t)]}\rangle\right|, \tag{5}$$

where the mean $\langle . \rangle$ could be either over an ensemble of many oscillators, which measures the phase coherence of the whole ensemble, or over time for a single pair of oscillators, in which case it measures the average coherence of that pair. A value of r close to zero indicates the absence of any coherence, while a value close to one indicates (almost) perfect coherence. Intermediate values indicate, that either not all oscillators within an ensemble are synchronized or, in the case of the mean over time, two oscillators are synchronized just for certain epochs.

The problem which usually arises is how to find a proper mapping from the state variable $\vec{x}$ to the phase φ. In the case in which a clear center of rotation can be found,

about that the system's trajectory rotates, a phase can be defined as the angle of the trajectory with respect to that center. Another approach, especially in the case when just one observable of $\vec{x}$ is accessible, is the use of the Hilbert transform [1], a tool borrowed from signal processing [48] which originated in complex analysis. By this approach an analytic signal can be constructed from which the phase can be extracted easily. In our paper [14] the Hilbert transform is computed implicitly by the wavelet transform and the use of an analytic (progressive) wavelet. We also use this tool in [15] to compute the phase of data acquired by experiments with electrical circuits.

Synchronization and multiple time-scales

Problems arise when no center of rotation exists or the system exhibits several oscillatory time-scales. In these cases the system's power spectrum is not band limited and it is not possible to extract the phase of a specific narrow frequency band. But, however, other approaches are possible to detect the phase synchronization without the need to define a phase.

Every attractor, which does not contain a fixed point, possesses at least one vanishing Lyapunov exponent [49]. This Lyapunov exponent corresponds to the free phase of the trajectory and can be explained by the fact that a perturbation within direction of the flow will on average remain constant throughout time. As one couples two oscillatory systems, each possessing one zero Lyapunov exponent, given that the interaction is sufficiently strong, one of the zero Lyapunov exponents will become negative. This is the onset of phase synchronization. The two coupled systems have just one free phase together and a perturbation of the phase of one of the subsystems will shrink throughout time, reflecting the attracting force between the phases [50]. By computing the Lyapunov spectrum it is possible to determine the onset of phase synchronization in a system of coupled oscillators. I used this technique in our paper [15] to verify that the phase synchronization found by the simple angular approach described above has correctly been identified. This was needed, since it was not obvious that the results obtained by the *naïve* phase approach are correct, due to the multiple time scales present it the analyzed system.

Phase synchronization of chaotic systems can also be explained in terms of their unstable periodic orbits. Embedded in a chaotic attractor lies a set of these unstable orbits which form a kind of *skeleton* of the attractor. When two chaotic oscillators are phase synchronized their unstable periodic orbits are locked [51]. Linked to the synchronization of the unstable orbits and, thus, the attractors is the coincidence of the recurrence times of the two systems. Several techniques have been developed that exploit this fact. These are, for instance, the "classical" stroboscopic observation for an periodically forced chaotic system [1], its expansion to mutually coupled chaotic oscillators described in [34], and another approach based on recurrence analysis [33].

In the case of phase synchronization the maxima of the return probabilities $P(\tau)$ (see Sec. 2.2) of two coupled systems will coincide due to the simultaneous returns of both system which are caused by the locked unstable periodic orbits. In our article [13] we extend this recurrence based technique to analyze phase synchronization among bursting neurons, which are systems exhibiting two predominant time scales. We study large networks of these neurons and report our findings, which is a diverse route to synchrony on the different time scales. In addition we discover a form of anomalous synchronization [52] which is only present in the fast time scale.

In our paper [14] we study synchronization in a system of two CO_2 lasers coupled via a master-slave coupling scheme. The synchronization scenario is complicated in that system. Both lasers are forced by an external sinusoidal signal and, hence, both are in perfect synchrony with that external force. However, due to the complicated multiple time scale dynamics active in that system, there is another, concealed, component in the dynamics, which can synchronize. Such a CO_2 laser system also exhibits a form of bursting pattern, which is different to those observed in neurons, though. These bursts are time intervals in which the trajectory spends a rather long time close to unstable periodic orbit of a certain length and amplitude which may differ drastically among the orbits. The observed synchronization of these high amplitude bursts can be explained in terms of unstable periodic orbits and the synchronization thereof. We analyzed the synchronization of these orbits utilizing the continuous wavelet transform and show that orbits of different length synchronize differently in dependence of the coupling strength.

Analytic treatment of synchronization

Synchronization phenomena can be treated analytically. Without going into much detail on topics, such as *route to chaos* and *bifurcation theory*, I just want to state some facts which are important for the reader in order to understand the analytically description of synchronization.

As mentioned above chaos can be understood in terms of a set of unstable periodic orbits (unstable limit cycles) building up the chaotic attractor. Limit cycles are created through a Hopf bifurcation, with respect to a control parameter. Any generic two-dimensional system undergoing a Hopf bifurcation can be transformed into the form [53, 54]:

$$\dot{u} \;=\; (\alpha + i)u - |u|^2 u + O(|u|^4). \tag{6}$$

Equation (6) is known as Hopf normal form. Here $u \in \mathbb{C}$ is the state variable and α is the Hopf bifurcation parameter. For $\alpha < 0$ the system has a stable fixed point at $u = 0$. When $\alpha = 0$ the Hopf bifurcation occurs, and for $\alpha > 0$ the former stable fixed point becomes unstable and a new stable limit cycle with radius $r = \sqrt{\alpha}$ appears.

Equation (6) is in a bit more generalized form also known as Stuart-Landau oscillator:

$$\dot{u} = (\alpha + i\omega)u - (1 + i\beta)|u|^2 u. \tag{7}$$

Here, a tunable frequency ω has been introduced and the *sheer* parameter β which controls isochronicity of the trajectories approaching the limit cycle. This equation is well studied in literature about synchronization, where systems of coupled Stuart-Landau oscillators are a simple paradigmatic model to analyze and understand synchronization phenomena analytically, since implications follow for more complex and chaotic systems as well.

However, oversimplifying a system may also destroy phenomena which could otherwise be observed in more realistic models. In [15] we study remote synchronization, that is mutual phase synchronization of two oscillator, which are coupled only indirectly via another oscillator which is not in synchrony with the former two. We are able to show that this phenomena, which is important in heterogeneous oscillatory networks, depends on the existence of a perturbable amplitude.

This has important implications. Consequently, we can show that oscillators without an amplitude, or precisely with a fixed not perturbable amplitude, are not able to reproduce remote synchronization. In particular, the popular and widely studied [47] Kuramoto phase oscillator is such a system. Nevertheless, this is only important in stronlgy heterogeneous oscillatory networks with a complex topology and broad frequency distribution. In such situation it is advisable not to use pure phase oscillators, since certain aspects of information transmission will be abolished by such systems. We demonstrate in [15] that the remote synchronization can be tracked by analyzing modulations in the instantaneous frequency of the oscillators. We also checked with the approach described in [34] that nonlinear methods are able to reveal the *hidden* information transfer through which the remotely synchronized oscillators communicate.

3 Conclusions

This present work has been focusing on synchronization, in particular phase synchronization, in systems exhibiting multiple time scales, which is still a rather untouched topic. Multiple time scales can be active in different manners within dynamical systems. Three different systems have been studied, each one having its own characteristic type of exhibiting multiple time scales.

The first system studied is a large heterogenous network of bursting neurons [13]. This system has been analyzed with methods based on recurrence in phase space. An interesting result are the different transitions to synchrony found in the two distinct time scales. Moreover, an anomalous synchronization effect can be observed in the fast spiking time scale.

The second system analyzed is a pair of coupled CO_2 lasers in a chaotic bursting regime [14]. This system is interesting due to its connection to epidemics [12]. We explain the bursts by different time scales generated from unstable periodic orbits em-

bedded in the attractor and perform a synchronization analysis of these different orbits utilizing the continuous wavelet transform. We find a diverse route to synchrony of these different observed time scales.

The last system studied is a small network motif of paradigmatic limit cycle oscillators [15]. Precisely, we have studied a hub motif, which serves as elementary building block for scale-free networks, a type of network found in many real world applications. These hubs are of special importance for communication and information transfer in complex networks. Here, a detailed study on the mechanism of synchronization in oscillatory networks with a broad frequency distribution has been carried out. In particular we find a remote synchronization of nodes in the network which are not directly coupled. We also explain the responsible mechanism and its limitations and constraints. Further, we derive an analytic expression for it and show that information transmission in pure phase oscillators, such as the Kuramoto type, is limited.

open questions and outlook

The observed anomalous synchronization in the fast time scale of the studied neuronal networks should be analyzed in more detail. In particular, a simpler system must be derived which can either relate to the mechanism described in [52] or may hint to another mechanism responsible for the observed phenomenon, which is a loss of phase coherence for intermediate values of the coupling strength.

The wavelet based method used in the study of the coupled laser system, should be applied to other systems as well. Also, an extension to detect n:m synchronization[6] might be interesting.

The study on remote synchronization has just started and seems promising. There are several ways how to continue the investigation of this. More complex topologies, such as two or more coupled hubs, or chains of oscillators can be introduced. Further, when increasing the complexity of the network's topology more different heterogeneities are possible. For instance the two similar nodes could be coupled via different paths, each path having different lengths and frequency distributions. Here, in particular the paths of information transmission within the network are of strong interest. Also such simple changes as complex coupling constants or introducing non-isochronicity in the oscillators may change a lot in the way the systems synchronizes within that complex time scale and topology mixture. Further, using more complicated systems (anharmonic limit cycles, chaotic, multiple time scales) as nodes may most likely introduce new effects, such as n:m synchronization.

[6] n:m synchronization is a generalized form of (4) to ratios of different frequencies: $|n\varphi_2(t) - m\varphi_1(t)| \leq \theta$.

Acknowledgements

First of all I would like to thank Jürgen Kurths for giving me the opportunity to do my PhD with him, for his financial support and for trusting me in doing my work autonomously.

I thank Riccardo Meucci for the nice collaboration I did with him and for his warm welcome of me and my family in Florence.

I'm giving my thanks to Luigi Fortuna, Mattia Frasca, Arturo Buscarino, and Gregorio Sciuto for the nice times I had with them in Catania and for the great team work from which our great paper has emerged.

Many thanks go to Matthias Holschneider for his great support, the scientific way of thinking I learned from him, the deep insights in wavelets I got through him and also for supporting me financially.

Great thanks go to Udo Schwarz for always helping me, being there to answer my questions and having time to discuss many scientific and philosophical ideas.

I would like thank Maria "Mamen" Carmen Romano and Marco Thiel for helping me in the begging in becoming a scientist and Joelle "Jojo" Ngamga for her support and helping a lot with many boring bureaucratic things.

I like to thank my colleagues Markus Abel, Karsten Ahnert, Mario Mulansky, and Grigory Bordyugov, for the many nice coffee breaks including scientific and non-scientific discussions which also helped a lot advancing in what I was doing and in what I am going to do.

I'd also like to give my thanks to the many different room mates I had throughout the years for nice discussions and a relaxed atmosphere; thanks to Tiago, Gunnar, Jonathan, Naoki, Natalia, Yernur and Azamat.

I am grateful to my family for all its support. Most of all I thank my lovely wife Helena for giving me all that time I needed and being so patient with me and of course my daughter Dalia and my son Filip for enlightening my life. I also would like to thank Helena's parents for babysitting so often and helping us a lot with everything all the time.

References

[1] **Synchronization - A universal concept in nonlinear science**
by A. Pikovsky, M. Rosenblum, J. Kurths *in* Cambridge University Press, 2001.

[2] **Synchronization of Lorenz-Based Chaotic Circuits with Applications to Communications**
by K. M. Cuomo, A. V. Oppenheim, S. H. Strogatz *in* IEEE Trans. on Circuits and Systems II, 40 (10), 1993.

[3] **Minimization of the energy flow in the synchronization of nonidentical chaotic systems**
by C. Sarasola, A. d'Anjou, F. J. Torrealdea, M. Graña *in* Phys. Rev. E, 72, 026223, 2005.

[4] **Synchronization of genetic oscillators**
by T. Zhou, J. Zhang, Z. Yuan, L. Chen *in* Chaos, 18, 037126, 2008.

[5] **Brain Dynamics: An Introduction to Models and Simulations**
by H. Haken *in* Springer-Verlag Berlin, 2002.

[6] **Synchronization in the human cardiorespiratory system**
by C. Schäfer, M. G. Rosenblum, H.-H. Abel, J. Kurths *in* Phys. Rev. E, 60 (1), 1999.

[7] **Spatio-temporal synchronization of recurrent epidemics**
by D. He, L. Stone *in* Proc. R. Soc. Lond. B, 270, 1519, 2003.

[8] **Pathological synchronization in Parkinson's disease: networks, models and treatments**
by C. Hammond, H. Bergman, P. Brown *in* Trends Neurosc., 30 (7), 2007.

[9] `http://en.wikipedia.org/wiki/Phase-locked_loop`

[10] **Chaotic Mimic Robots**
by A. Buscarino, C. Camerano, L. Fortuna, M. Frasca *in* Phil. Trans. R. Soc. A, 368, 2179, 2010.

[11] **Handbook of Chaos Control**
by E. Schöll, H. G. Schuster (Eds.) *in* Wiley-VCH, 2007.

[12] **Stochastic epidemic outbreaks: why epidemics are like lasers**
by Ira B. Schwartz, Lora Billings *in* Proceedings of SPIE, 5471, 2004.

[13] **Synchronization Analysis of Neuronal Networks by Means of Recurrence Plots**
by A. Bergner, M. C. Romano, J. Kurths, M. Thiel *in* "Lectures in Supercomputational Neuroscience", Springer-Verlag Berlin Heidelberg, pp. 177, 2008.

[14] **Continuous wavelet transform in the analysis of burst synchronization in a coupled laser system**
by A. Bergner, R. Meucci, K. Al Naimee, M. C. Romano, M. Thiel, J. Kurths, F. T. Arecchi *in* Phys. Rev. E, 78, 016211, 2008.

[15] **Remote Synchronization in Complex Networks**
by A. Bergner, M. Frasca, G. Sciuto, A. Buscarino, E.J. Ngamga, L. Fortuna, J. Kurths *in* Phys. Rev. E, *submitted*.

[16] **Collective dynamics of 'small-world' networks**
by D. J. Watts, S. H. Strogatz *in* Nature, 393, 440, 1998.

[17] **Emergence of Scaling in Random Networks**
by A.-L. Barabási, R. Albert *in* Science, 286, 1999.

[18] **Complexity: a guided tour**
by M. Mitchell *in* Oxford University Press, 2009.

[19] **Statistical mechanics of complex networks**
by R. Albert, A.-L. Barabási *in* Rev. mod. Phy., 74, 2002.

[20] **Complex networks: Structure and dynamics**
by S. Boccaletti, V. Latorab, Y. Morenod, M. Chavezf, D.-U. Hwanga *in* Physics Reports, 424, 175, 2006.

[21] **Synchronization in Oscillatory Networks**
by G. V. Osipov, J. Kurths, C. Zhou *in* Springer-Verlag Berlin, 2007.

[22] **Synchronization in complex networks**
by A. Arenas, A. Díaz-Guilera, J. Kurths, Y. Moreno, C. Zhou *in* Physics Reports, 469, 93-153, 2008.

[23] **Networks on the edge of chaos: Global feedback control of turbulence in oscillator networks**
by S. Gil, A. S. Mikhailov *in* Phys. Rev. E, 79, 026219, 2009.

[24] **Oscillatory Neurocomputers with Dynamic Connectivity**
by F. C. Hoppensteadt, E. M. Izhikevich *in* Phys. Rev. Lett., 82 (14), 1999.

[25] `http://scholar.google.com/scholar?q=oscillator+network+application`

[26] **Network Motifs: Simple Building Blocks of Complex Networks**
by R. Milo, S. Shen-Orr, S. Itzkovitz, N. Kashtan, D. Chklovskii, U. Alon *in* Science, 298, 2002.

[27] `http://de.wikipedia.org/wiki/Ewige_Wiederkunft`
`http://en.wikipedia.org/wiki/Eternal_return`

[28] **Sur la probleme des trois corps et les 'equations de la dynamique**
by H. Poincaré *in* Acta Mathematica, 13, 1-271, 1890.

[29] **Recurrence Plots for the Analysis of Complex Systems**
by N. Marwan, M. C. Romano, M. Thiel, J. Kurths *in* Phys. Rep., 438, 237-329, 2007.

[30] **Recurrence Plots of Dynamical Systems**
by J.-P. Eckmann, S. O. Kamphorst, D. Ruelle *in* Europhys. Lett., 5, 973-977, 1987.

[31] **Nonlinear Time Series Analysis**
by H. Kantz, T. Schreiber *in* Cambridge University Press, 2003.

[32] **Recurrence networks–a novel paradigm for nonlinear time series analysis**
by R. V. Donner, Y. Zou, J. F. Donges, N. Marwan, J. Kurths *in* New J. Phys. 12, 033025, 2010.

[33] **Detection of synchronization for non-phase-coherent and non-stationary data**
by M. C. Romano, M. Thiel, J. Kurths, I. Z. Kiss, J. L. Hudson *in* Europhys. Lett., 71 (3), 466, 2005.

[34] **General framework for phase synchronization through localized sets**
by T. Pereira, M. S. Baptista, J. Kurths *in* Phys. Rev. E, 75, 026216, 2007.

[35] `http://www.newworldencyclopedia.org/entry/Joseph_Fourier`

[36] `http://en.wikipedia.org/wiki/Gabor_atom`

[37] **Theory of Communication**
by D. Gabor *in* J. Inst. Electr. Eng., 93, 1946.

[38] **Wave propagation and sampling theory-Part I: Complex signal and scattering in multilayered media**
by J. Morlet, G. Arens, E. Fourgeau, D. Glard *in* Geophysics, 47 (2), 203-221, 1982.

[39] **Wavelets: an analysis tool**
by M. Holschneider *in* Oxford University Press, 1995.

[40] **A Wavelet Tour of Signal Processing**
by S. Mallat *in* Academic Press, 1999.

[41] **Signal Analysis: Wavelets, Filter Banks, Time-Frequency Transforms and Applications**
by A. Mertins *in* Wiley, 1999.

[42] **The empirical mode decomposition and the Hilbert spectrum for nonlinear and non-stationary time series analysis**
by N. E. Huang, Z. Shen, S. R. Long, M. C. Wu, H. H. Shih, Q. Zheng, N.-C. Yen, C.C. Tung, H. H. Liu *in* Proc. R. Soc. Lond. A, 454, 903-995, 1998.

[43] **Matching Pursuits with Time-Frequency Dictionaries**
by S. G. Mallat, Zhifeng Zhang *in* IEEE Trans. Sig. Proc., 3397-3415, 1993.

[44] **Generalized synchronization of chaos in directionally coupled chaotic systems**
by N.F. Rulkov, M.M. Suschik, L.S. Tsimring, H.D.I. Abarbanel *in* Phys. Rev. E, 51, 980, 1995.

[45] **From Phase to Lag Synchronization in Coupled Chaotic Oscillators**
by M. G. Rosenblum, A. S. Pikovsky, J.Kurths *in* Phys. Rev. Lett. 78, 22, 1997.

[46] **Chemical Oscillations, Waves, and Turbulence**
by Y. Kuramoto *in* Springer-Verlag Berlin Heidelberg, 1984.

[47] **The Kuramoto model: A simple paradigm for synchronization phenomena**
by J. A. Acebrón, L. L. Bonilla, C. J. Pérez Vicente, F. Ritort, R. Spigler *in* Rev. Mod. Phys., 77, 137-185, 2005.

[48] **Signals and Systems**
by B. Girod, R. Rabenstein, A. Stenger *in* Wiley, 2001.

[49] **At least one Lyapunov exponent vanishes if the trajectory of an attractor does not contain a fixed point**
by H. Haken *in* Phys. Lett. A, 94 (2), 71-72, 1983.

[50] **Phase Synchronization of Chaotic Oscillators**
by M. Rosenblum, A. Pikovsky, J. Kurths *in* Phys. Rev. Lett., 76, 11, 1804-1807, 1996.

[51] **Role of unstable periodic orbits in phase and lag synchronization between coupled chaotic oscillators**
by D. Pazó, M. A. Zaks, J. Kurths *in* Chaos, 13, 1, 2003.

[52] **Anomalous phase synchronization in populations of nonidentical oscillators**
by B. Blasius, E. Montbrió, J. Kurths *in* Phys. Rev. E, 67, 035204(R), 2003.

[53] **Elements of Applied Bifurcation Theory, 2nd Edition**
by Yuri A. Kuznetsov *in* Springer-Verlag, 1998.

[54] **Amplitude response of coupled oscillators**
by D.G. Aronson, G.B. Ermentrout, N. Kopell *in* Physica D, 41, 403-449, 1990.

A Publications

A.1 Synchronization Analysis of Neuronal Networks by Means of Recurrence Plots

The book chapter *Synchronization Analysis of Neuronal Networks by Means of Recurrence Plots* has been published as part of *Lectures in Supercomputational Neuroscience* in Springer-Verlag Berlin Heidelberg, pages 177–191, in 2008. I acknowledge the rights for republication within my thesis.

6

Synchronization Analysis of Neuronal Networks by Means of Recurrence Plots

André Bergner and Maria Carmen Romano, Jürgen Kurths and Marco Thiel

Nonlinear Dynamics Group, University of Potsdam
bergner@agnld.uni-potsdam.de

Summary. We present a method for synchronization analysis, that is able to handle large networks of interacting dynamical units. We focus on large networks with different topologies (random, small-world and scale-free) and neuronal dynamics at each node. We consider neurons that exhibit dynamics on two time scales, namely spiking and bursting behavior. The proposed method is able to distinguish between synchronization of spikes and synchronization of bursts, so that we analyze the synchronization of each time scale separately. We find for all network topologies that the synchronization of the bursts sets in for smaller coupling strengths than the synchronization of the spikes. Furthermore, we obtain an interesting behavior for the synchronization of the spikes dependent on the coupling strength: for small values of the coupling, the synchronization of the spikes increases, but for intermediate values of the coupling, the synchronization index of the spikes decreases. For larger values of the coupling strength, the synchronization index increases again until all the spikes synchronize.

6.1 Introduction

Networks are ubiquitous in nature, biology, technology and in the social sciences (see [1] and references therein). Much effort has been made to describe and characterize them in different fields of research. One key finding of these studies is that there are unifying principles underlying their behavior. In the past, two major approaches have been pursued to deal with networks. The first approach considers networks of regular topology, such as arrays or rings of coupled systems with nonlinear and complex dynamics on each node. The second approach concentrates on the topology of the network and sets aside the dynamics or at most considers a rather simple one at each node. Some of the prototypical types of network architectures that have been considered are random, small-world, scale-free and generalized random networks [2].

Recently, the study of complex dynamics on the nodes has been extended from regular to more complex architectures [3]. However, in most previous

work, each node is still considered to be a phase oscillator (system with one predominant time scale), often pulse-coupled to each other. Much is left, however, to understand about network behavior with more realistic complex dynamics on the nodes of networks of complex architecture, such as chaotic and stochastic dynamics, which is found in many real application systems, such as in neural networks. The influence of the topology of the network on the dynamical properties of the complex systems is currently being investigated in the context of synchronisation [4–6].

Synchronization of complex systems has been intensively studied during the last years [7] and it has been found to be present in numerous natural and engineering systems [8]. Chaotic systems defy synchronization due to their sensitivity to slight differences in initial conditions. However, it has been demonstrated that these kind of systems are able to synchronize. In the case of two interacting non-identical chaotic systems (which is more likely to occur in nature than if they were identical), several types of synchronization might occur, dependent on the coupling strength between the systems. For rather weak coupling strength, phase synchronisation (PS) might set in. In this case, the phases and frequencies of the complex systems are locked, i.e. $|\phi_1(t) - \phi_2(t)| < \text{const.}$ and $\omega_1 \approx \omega_2$, whereas their amplitudes remain uncorrelated. If the coupling strength is further increased, a stronger relationship between the interacting systems might occur, namely generalized synchronization (GS). In this case, there is a functional relationship between both systems. Finally, for very strong coupling, both systems can become almost completely synchronized. Then, their trajectories evolve almost identically in time [7].

In the case of phase synchronization, the first step in the analysis is to determine the phases $\phi_1(t)$ and $\phi_2(t)$ of the two interacting systems with respect to the time t. If the chaotic systems have mainly one characteristic time scale, i.e. a predominant peak in the power spectrum, the phase can be estimated as the angle of rotation around one center of the projection of the trajectory on an appropriate plane. Alternatively, the analytical signal approach can be used [9]. However, for most of the complex systems found in nature, there is more than one characteristic time scale [10]. Hence, the approaches mentioned above to estimate the phase are not appropriate. Recently, a new method, based on the recurrence properties of the interacting systems [11], has been introduced to overcome this problem. By means of this technique, it is possible to analyze systems with a rather broad spectrum, as well as systems strongly contaminated by noise or subjected to non-stationarity [12].

In this chapter, we extend the recurrence based technique for phase synchronization analysis to systems with two predominant time scales, so that it is possible to obtain one synchronization index for each time scale. Moreover, we apply this method to large networks of different architectures with neuronal dynamics on their nodes.

The outline of this chapter is as follows: in Sect. 6.2, we introduce the concept of recurrence, as well as the synchronization index based on the recurrence

properties of the system. In Sect. 6.2.2, we present the method to analyze the synchronization for two different time scales separately. In Sect. 6.3, we apply the method to complex networks of neurons and present the obtained results.

6.2 Phase Synchronization by Means of Recurrences

First, we show the problem of defining the phase in systems with rather broad power spectrum by using the paradigmatic system of two coupled non-identical Rössler oscillators:

$$\begin{aligned} \dot{x}_{1,2} &= -\omega_{1,2} y_{1,2} - z_{1,2} \\ \dot{y}_{1,2} &= \omega_{1,2} x_{1,2} + a y_{1,2} + \mu(y_{2,1} - y_{1,2}) \\ \dot{z}_{1,2} &= 0.1 + z_{1,2}(x_{1,2} - 8.5) \,, \end{aligned} \tag{6.1}$$

where μ is the coupling strength and $\omega_{1,2}$ determine the mean intrinsic frequency of the (uncoupled) oscillators in the case of phase coherent attractors. In our simulations, we take $\omega_1 = 0.98$ and $\omega_2 = 1.02$. The parameter $a \in [0.15, 0.3]$ governs the topology of the chaotic attractor. When a is below a critical value a_c ($a_c \approx 0.186$ for $\omega_1 = 0.98$ and $a_c \approx 0.195$ for $\omega_2 = 1.02$), the chaotic trajectories always cycle around the unstable fixed point $(x_0, y_0) \approx (0, 0)$ in the (x, y) subspace (Fig. 6.1(a)). In this case, the rotation angle

$$\phi = \arctan \frac{y}{x} \tag{6.2}$$

can be defined as the phase which increases almost uniformly. The oscillator has coherent phase dynamics, i.e. the diffusion of the phase dynamics is very low (10^{-5}–10^{-4}). In this case, other phase definitions, e.g. based on the Hilbert transform or on the Poincaré section, yield equivalent results [9]. However, beyond the critical value a_c, the trajectories no longer completely cycle around (x_0, y_0) – the attractor becomes the so-called funnel attractor. Such earlier returns in the funnel attractor happen more frequently with increasing a (Fig. 6.1(b)). It is clear that for the funnel attractors, usual (and rather simple) definitions of phase, such as (6.2), are no longer applicable [9].

Another problematic case arises if the systems under consideration have two predominant time scales, which is common in many real systems, e.g. neurons with spiking and bursting dynamics. In such cases, the definition of the phase given by (6.2) is also not appropriate.

Figure 6.2 shows these problems with the time series of a Hindmarsh-Rose neuron.[1]

Rosenblum et al. [13] have proposed the use of an ensemble of phase coherent oscillators that is driven by a non-phase-coherent oscillator in order to estimate the frequency of the latter and hence detect PS in such kind

[1] For the definition of the Hindmarsh-Rose neuron see Sect. 6.3 and also Chap. 1.

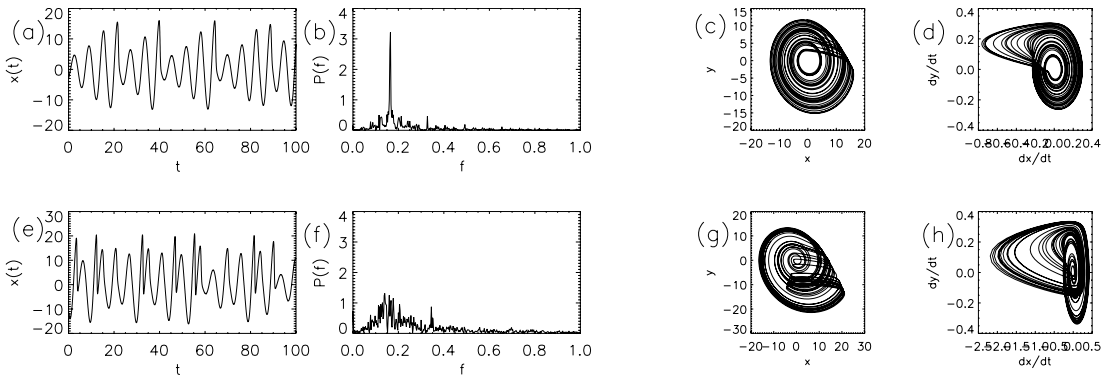

Fig. 6.1. (**a,e**): Segment of the x_1-component of the trajectory of the Rössler systems (6.1); (**b,f**): periodogram of the x-component of the trajectory; (**c,g**): projection of the attractor onto the (x, y) plane; (**d,h**): projection onto the $(\dot{x}, \dot{y})$ plane. Upper panel (**a,b,c,d**) computed for $a = 0.16$ and lower panel (**e,f,g,h**) computed for $a = 0.2925$

of systems. However, depending on the component one uses to couple the non-phase-coherent oscillator to the coherent ones, the result of the obtained frequency can be different.

Furthermore, Osipov et al. [10] have proposed another approach which is based on the general idea of the curvature of an arbitrary curve. For any two-dimensional curve $\boldsymbol{r} = (u, v)$ they propose that the phase ϕ be defined as $\phi = \arctan \frac{\dot{v}}{\dot{u}}$. By means of this definition, the projection $\dot{\boldsymbol{r}} = (\dot{u}, \dot{v})$ is a curve cycling monotonically around a certain point.

This definition of ϕ holds in general for any dynamical system if the projection of the phase trajectory onto some plane is a curve with a positive curvature. This approach is applicable to a large variety of chaotic oscillators, such as the Lorenz system [14], the Chua circuit [15] or the model of an ideal four-level laser with periodic pump modulation [16].

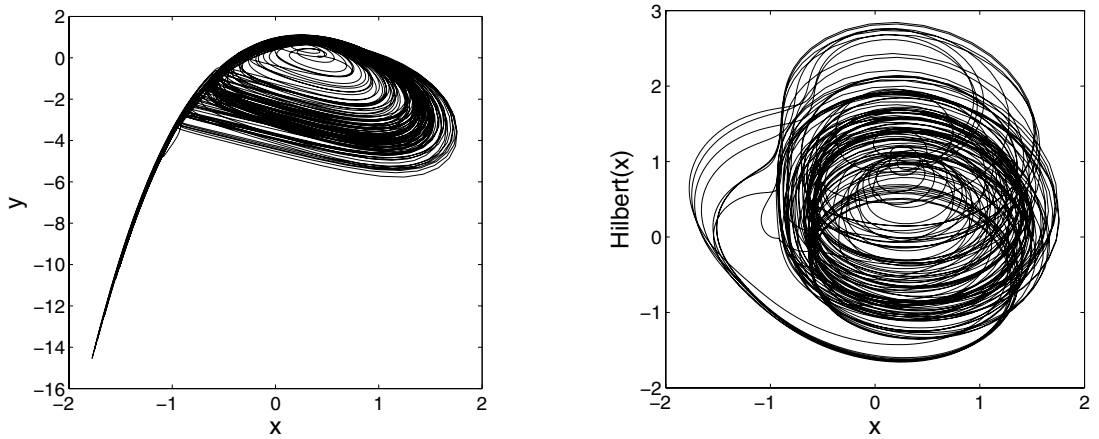

Fig. 6.2. Projection of the x-y-plane; (**a**) and the plot of the Hilbert Transform of x versus x; (**b**) for the Hindmarsh-Rose-neuron

This is clear for phase-coherent as well as funnel attractors in the Rössler oscillator. Here, projections of chaotic trajectories on the plane $(\dot{x}, \dot{y})$ always rotate around the origin (Figs. 6.1(c) and (d)) and the phase can be defined as

$$\phi = \arctan \frac{\dot{y}}{\dot{x}} \ . \tag{6.3}$$

Although this approach works well in non-phase-coherent model systems, we have to consider that one is often confronted with the computation of the phase in experimental time series, which are usually corrupted by noise. In this case, some difficulties may appear when computing the phase given in (6.3), because derivatives are involved in its definition.

6.2.1 Cross-correlation of the Probability of Recurrence

We use a different approach, based on recurrences in phase space, to detect PS indirectly. We define a recurrence of the trajectory of a dynamical system $\{\boldsymbol{x}_i\}_{i=1}^N$ in the following way: we say that the trajectory has returned at time $t=j$ to the former point in phase space visited at $t=i$ if

$$R_{i,j}^{(\varepsilon)} = \Theta(\varepsilon - \|\boldsymbol{x}_i - \boldsymbol{x}_j\|) = 1 \ , \tag{6.4}$$

where ε is a pre-defined threshold and $\Theta(\cdot)$ is the Heaviside function. A "1" in the matrix at i, j means that $\boldsymbol{x}_i$ and $\boldsymbol{x}_j$ are neighboring, a "0" that they are not. The black and white representation of this binary matrix is called a recurrence plot (RP). This method has been intensively studied in the last years [11]: different measures of complexity have been proposed based on the structures obtained in the RP and have found numerous applications for example, in physiology and earth science [17]. Furthermore, it has been even shown that some dynamical invariants can be estimated by means of the recurrence structures [18].

Based on this definition of recurrence, one is able to tackle the problem of performing a synchronization analysis in the case of non-phase-coherent systems. We avoid the direct definition of the phase and use instead the recurrence properties of the systems in the following way: the probability $P^{(\varepsilon)}(\tau)$ that the system returns to the neighborhood of a former point $\boldsymbol{x}_i$ of the trajectory[2] after τ time steps can be estimated as follows:

$$P^{(\varepsilon)}(\tau) = \frac{1}{N-\tau} \sum_{i=1}^{N-\tau} \Theta(\varepsilon - \|\boldsymbol{x}_i - \boldsymbol{x}_{i+\tau}\|) = \frac{1}{N-\tau} \sum_{i=1}^{N-\tau} R_{i,i+\tau}^{(\varepsilon)} \ . \tag{6.5}$$

This function can be regarded as a generalized autocorrelation function, as it also describes higher order correlations between the points of the trajectory

[2] The neighborhood is defined as a box of size ε centered at $\boldsymbol{x}_i$, as we use the maximum norm.

dependent on the time delay τ. A further advantage with respect to the linear autocorrelation function is that $P^{(\varepsilon)}(\tau)$ is defined for a trajectory in phase space and not only for a single observable of the system's trajectory.

For a periodic system with period T, it can be easily shown that $P^{(\varepsilon)}(\tau)=1$ if $\tau = T$ and $P^{(\varepsilon)}(\tau) = 0$ otherwise. For coherent chaotic oscillators, such as (6.1) for $a=0.16$, $P^{(\varepsilon)}(\tau)$ has well-expressed local maxima at multiples of the mean period, but the probability of recurrence after one or more rotations around the fixed point is less than one (Fig. 6.3(b,d)).

Analyzing the probability of recurrence, it is possible to detect PS for non-phase-coherent oscillators as well. This approach is based on the following idea: Originally, a phase ϕ is assigned to a periodic trajectory $\boldsymbol{x}$ in phase space, by projecting the trajectory onto a plane and choosing an origin, around which the trajectory oscillates all the time. Then, an increment of 2π is assigned to ϕ when the point of the trajectory has returned to its starting position, i.e. when $\|\boldsymbol{x}(t+T) - \boldsymbol{x}(t)\| = 0$. Analogously to the case of a periodic system,

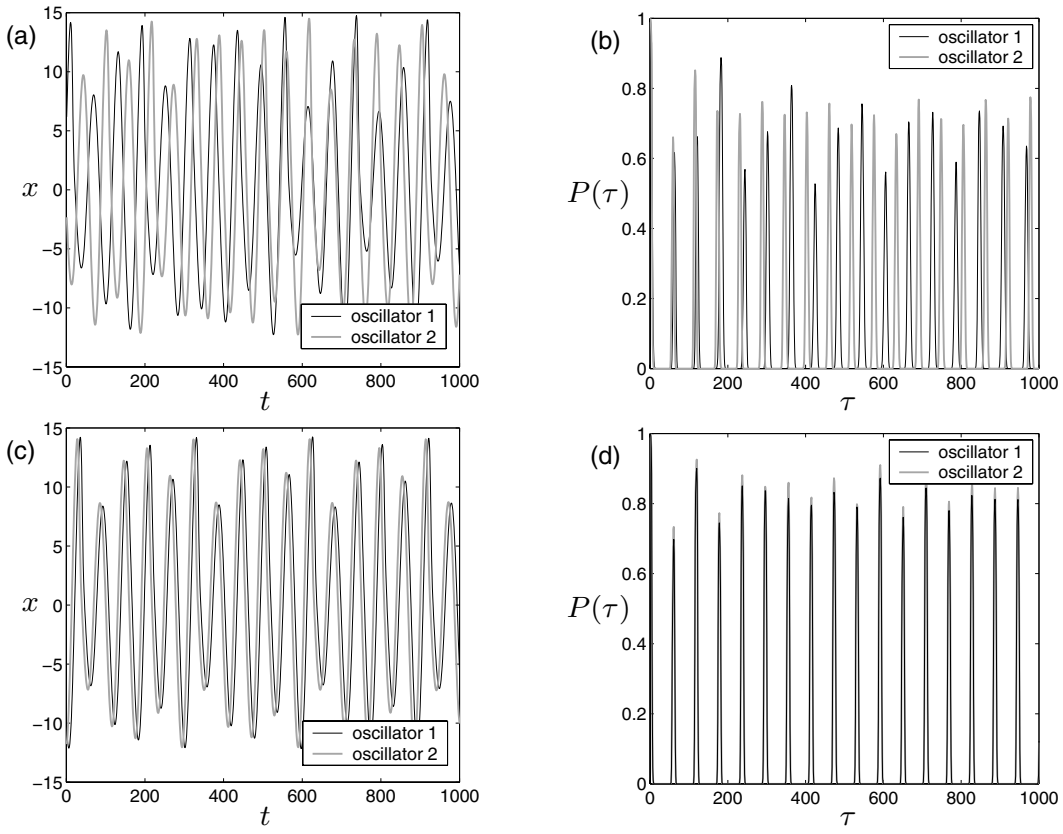

Fig. 6.3. Time series (**a** and **c**) and the probability of recurrence (**b** and **d**) of the Rössler system with parameters $a = 0.15$, $b = 0.2$, $c = 8.5$, $\omega_1 = 1$ and $\omega_2 = 1.05$. The coupling strength for the non-PS case (**a** and **b**) is $\mu_{\mathrm{nonPS}} = 0.01$ and $\mu_{\mathrm{PS}} = 0.07$ for the PS case (**c** and **d**), respectively. The values for CPR that have been calculated are $\mathrm{CPR}_{\mathrm{nonPS}} = 0.0102$ and $\mathrm{CPR}_{\mathrm{PS}} = 0.9995$. The figures show clearly how the peaks drift apart from each other in the absence of PS and coincide in the case of PS

we can assign an increment of 2π to ϕ for a complex non-periodic trajectory $\boldsymbol{x}(t)$ when $\|\boldsymbol{x}(t+T)-\boldsymbol{x}(t)\| \sim 0$, or equivalently when $\|\boldsymbol{x}(t+T)-\boldsymbol{x}(t)\| < \varepsilon$, where ε is a predefined threshold. That means that a recurrence $R^{(\varepsilon)}_{t,t+\tau} = 1$ can be interpreted as an increment of 2π of the phase in the time interval τ.[3]

$P^{(\varepsilon)}(\tau)$ can be viewed as a statistical measure of how often ϕ in the original phase space has increased by 2π or multiples of 2π within the time interval τ. If two systems are in PS, on the average, the phases of both systems increase by $2\pi\, k$, with k a natural number, within the same time interval τ. Hence, looking at the coincidence of the positions of the maxima of $P^{(\varepsilon)}(\tau)$ for both systems, we can quantitatively identify PS (from now on, we omit (ε) in $P^{(\varepsilon)}(\tau)$ to simplify the notation). The proposed algorithm then consists of two steps:

- Compute $P_{1,2}(\tau)$ of both systems based on (6.5).
- Compute the cross-correlation coefficient between $P_1(\tau)$ and $P_2(\tau)$ (Correlation between probabilities of recurrence)

$$\mathrm{CPR}_{1,2} = \frac{\left\langle \bar{P}_1(\tau)\bar{P}_2(\tau)\right\rangle_\tau}{\sigma_1\sigma_2}\,, \tag{6.6}$$

  where the bar above $\bar{P}_{1,2}$ denotes that the mean value has been subtracted and σ_1 and σ_2 are the standard deviations of $P_1(\tau)$ and $P_2(\tau)$, respectively.

If both systems are in PS, the probability of recurrence is maximal simultaneously and $\mathrm{CPR}_{1,2} \approx 1$. In contrast, if the systems are not in PS, the maxima of the probability of recurrence do not occur jointly and we would expect low values of $\mathrm{CPR}_{1,2}$.

In Figs. 6.3 and 6.4, we illustrate the performance of the method with two examples of the Rössler system.

6.2.2 The Problem of Separating the Time Scales

As already mentioned, neurons can exhibit dynamics on several distinct time scales (spiking and bursting) and are also able to synchronize on both scales separately. To perform a synchronisation analysis of such a system, one has to segregate the two scales of each other. Figure 6.5 shows the RP of a Hindmarsh-Rose neuron.[4] In Fig. 6.5(a), the structures that emerged from the recurrence of the bursts can be identified quite clearly, namely the "swelling diagonal lines". In Fig. 6.5(b), one of those "swellings" is presented magnified. Here, the recurrences of the spike dynamics can be noticed as diagonal lines on a smaller scale in the RP.

Separating the scales is a non-trivial task. Filtering the time series could be one approach, but this is not recommended as the attractor of the filtered time series will be distorted, which will change the recurrence behavior.

[3] This can be considered as an alternative definition of the phase to (6.2) and (6.3).
[4] For the definition of the Hindmarsh-Rose neuron see Sect. 6.3 and Chap. 1, again.

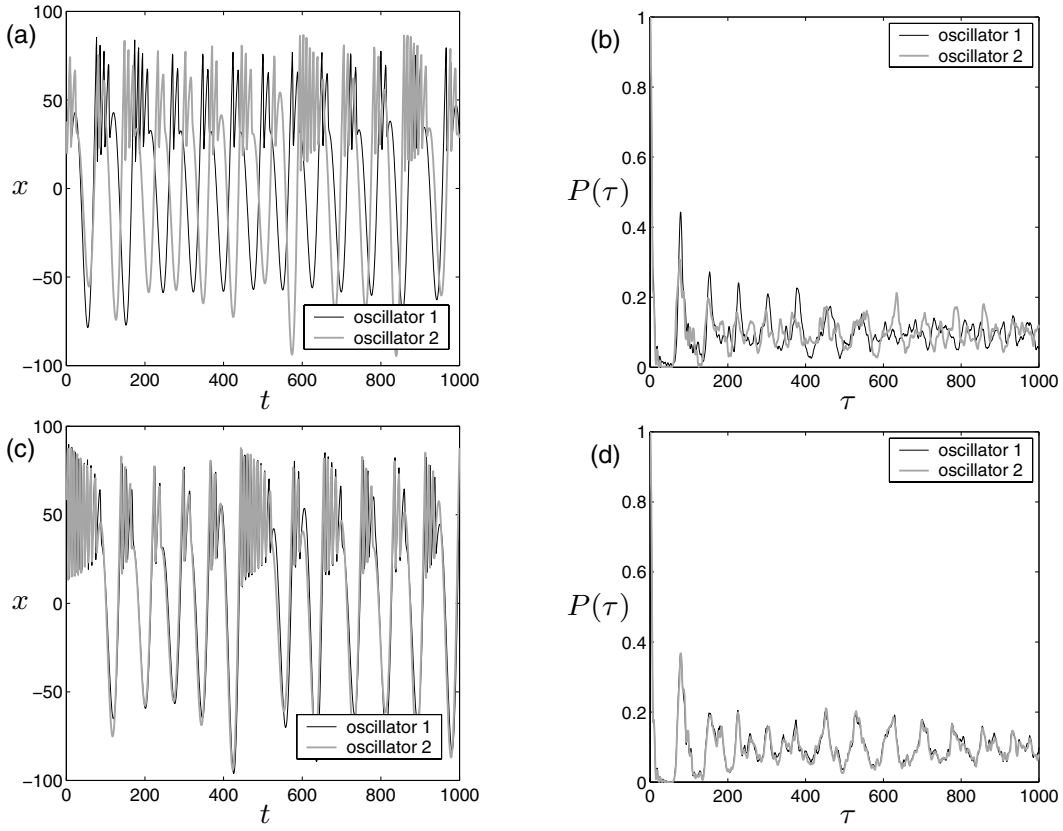

Fig. 6.4. Time series (**a** and **c**) and the probability of recurrence (**b** and **d**) of the Rössler system in a bursting regime with the parameters $a=0.38$, $b=0.4$, $c=50$, $\omega_1=1$ and $\omega_2=1.05$. The coupling strength for the non PS case (**a** and **b**) is $\mu_{\mathrm{nonPS}}=0.005$ and $\mu_{\mathrm{PS}}=0.23$ for the PS case (**c** and **d**), respectively. The values for CPR that have been calculated are $\mathrm{CPR}_{\mathrm{nonPS}}=0.0258$ and $\mathrm{CPR}_{\mathrm{PS}}=0.9684$. Clearly, the peaks do not coincide in the non-PS case and do so in the presence of PS. This example shows quite well that the algorithm is able to detect PS for systems with a very complicated flow of the phase

Therefore, separating the time scales after calculating the RP or $P(\tau)$ is a better approach. We separate the time scales in two ways: The first one requires the choice of an appropriate recurrence rate and the second one is the application of some filter to $P(\tau)$.

In Fig. 6.6(a) the recurrence probability $P(\tau)$ of a Hindmarsh-Rose neuron is presented. The large peaks correspond to the recurrence of the bursts. The arrows indicate the smaller peaks generated by the recurrence of the spikes. There are many methods for separating both scales, e.g. wavelets, etc. In this analysis, an infinite impulse response (IIR) filter has been used, which can be implemented easily by simple difference equations.

Figure 6.6(b) shows the highpass filtered $P(\tau)$. The cutoff has been chosen to be $0.2\times$ sampling rate. The broad peaks, originated by the burst, are filtered out and the smaller peaks corresponding to the spike recurrence become clearer. Note that the filtered $P(\tau)$ cannot be interpreted as a probability of

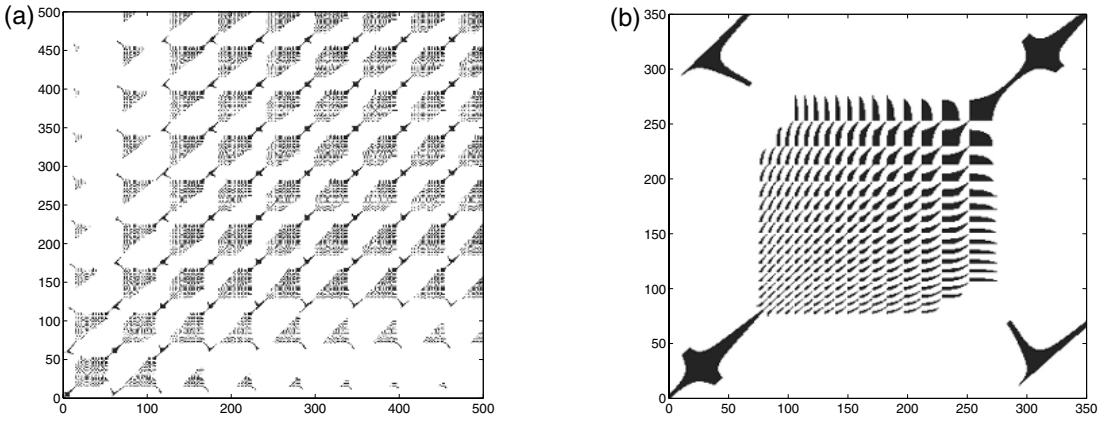

Fig. 6.5. Recurrence plot of the time series of a Hindmarsh-Rose neuron on a large scale (**a**) and zoomed in to show a small scale features (**b**)

recurrence any more, since it also assumes negative values. However, it still captures all the relevant information about the recurrence of the spiking dynamics. Thus, a separate synchronization analysis of the spike scale can now be accomplished by computing the index CPR of the filtered functions.

The recurrence rate is the parameter that specifies the number of black points in the RP and determines the threshold ε in (6.4). This parameter also influences the patterns obtained in the recurrence plot. Hence, by varying the recurrence rate, we can enhance or suppress certain information.

Figure 6.7(a) shows the RP of a Hindmarsh-Rose neuron time series, computed for a high recurrence rate of 0.5. Comparing this plot with the one in Fig. 6.5(a), it can be observed that the shorter lines originating from the recurrence of the spikes are "smeared out" The corresponding probability of recurrence $P(\tau)$ in Fig. 6.7(b) shows only the oscillations that are caused by

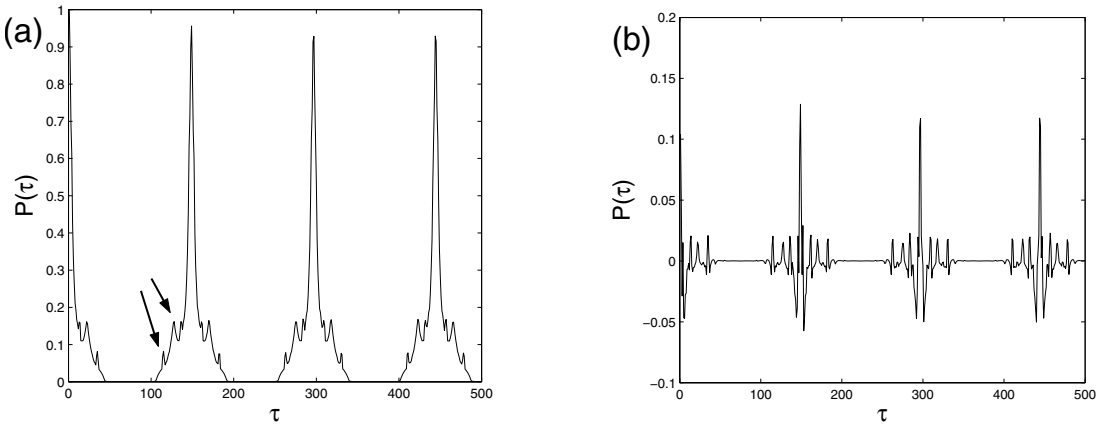

Fig. 6.6. Probability of recurrence $P(\tau)$ for the Hindmarsh-Rose neuron: (**a**) The original and; (**b**) highpass filtered. The arrows indicate the features created by the recurrence of the spikes

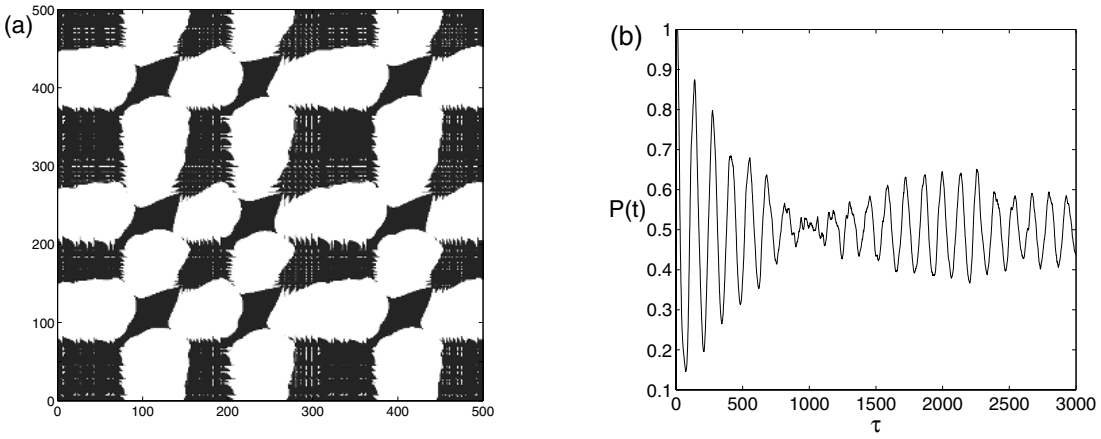

Fig. 6.7. RP with $RR = 0.5$; (**a**) and corresponding $P(\tau)$; (**b**) for an exemplary Hindmarsh-Rose neuron

the recurrence of the bursts. Consequently, the recurrence rate can be used to analyze the synchronization of the slow time scale (bursts), since the influence of the fast scale is automatically removed.

Analogously, choosing a rather low value for the recurrence rate causes the fine structures of the spike recurrences to appear more clearly. Therefore, it is advisable to use a rather low recurrence rate to analyze the synchronization of the spikes. In Fig. 6.8, the RP and the corresponding high-pass filtered $P(\tau)$ are presented. This example demonstrates quite well, how the large peaks, which are usually created by the recurrence of the bursts, are suppressed, so that the recurrence of the spikes is clearer than for higher values of the recurrence rate.

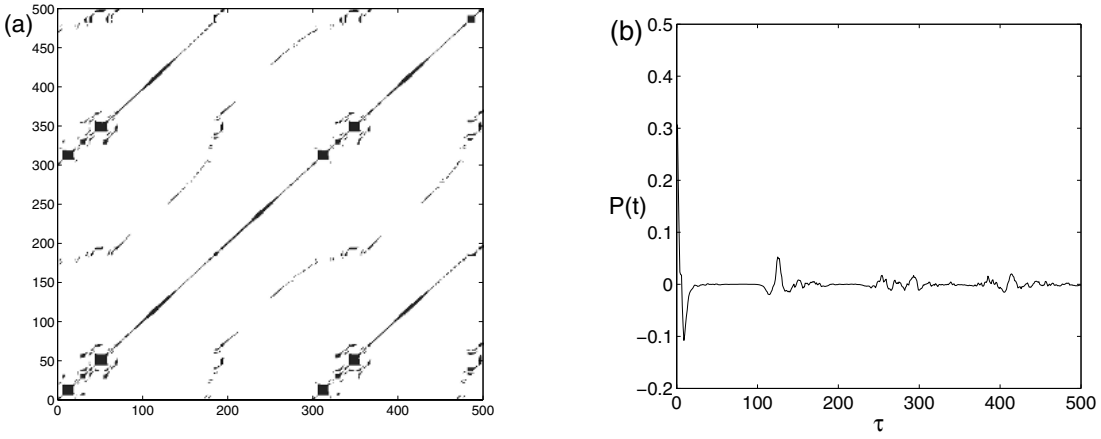

Fig. 6.8. RP with $RR = 0.05$: (**a**) and corresponding highpass filtered $P(\tau)$; (**b**) for an exemplary Hindmarsh-Rose neuron

A Few Notes on the Parameters

The RP based method has several parameters that need to be chosen in an appropriate way. These parameters are the already discussed recurrence rate and cutoff frequency of the filter, the averaging length N in (6.5), and the maximum recurrence time $\tau_{\max}$ when calculating CPR.

On the one hand, small values of N and $\tau_{\max}$ are desirable, such that the analysis can operate as locally as possible and with as small as possible computational cost. On the other hand, the values cannot be too small, since the analyses requires averaging and thus needs a large number of points for a correct calculation. Therefore, one has to determine the minimum values of N and $\tau_{\max}$ to serve both requirements. This can be done by calculating CPR for different values of these parameters. For large values, one can expect some kind of asymptotic behavior.

6.3 Application of the Algorithm

In this section, we present a few results that have been obtained by applying the proposed algorithm to networks of coupled neurons with different topologies. The neuron model that has been used is a (modified) four-dimensional Hindmarsh-Rose system (for details, see [19] and [20]),

$$\begin{aligned}
\dot{x}_n &= \omega_{\text{fast},n}(y_n + 3x_n^2 - x_n^3 - 0.99z_n + I_n) + \mu \textstyle\sum_{m=1}^{N} A_{nm}(x_m - x_n) \\
\dot{y}_n &= \omega_{\text{fast},n}(1.01 - y_n - 5.0128x_n^2 - 0.0278w_n) \\
\dot{z}_n &= \omega_{\text{slow1},n}(-z_n + 3.966(x_n + 1.605)) \\
\dot{w}_n &= \omega_{\text{slow2},n}(-0.9573w_n + 3(y_n + 1.619)),
\end{aligned} \tag{6.7}$$

where x_n is the membrane potential, and y_n, z_n, and w_n represent inner degrees of freedom of neuron n, with $n=1,\ldots,N$. Whereas y_n is responsible for the fast dynamics of the spikes, z_n and w_n represent the slow dynamics of the bursts. I_n is the external input current of neuron n, $\omega_{\text{fast},n}$ determines the firing rate, and $\omega_{\text{slow1},n}$ and $\omega_{\text{slow2},n}$ determine the duration of the bursts. The neurons are electrically coupled, while the coupling topology of the neurons is given by the adjacency matrix A_{nm} (see Chap. 3). The parameter μ is the coupling strength of the whole network.

6.3.1 Analysis of Two Coupled Neurons

First, we apply the algorithm to a pair of coupled Hindmarsh-Rose neurons. We consider different parameter sets for the two neurons (see Table 6.1), so that we have three possibilities for the dynamical regime of the neurons: (i) both neurons in regular bursting regime with different frequencies, (ii) both neurons in chaotic bursting regime with different frequencies, and (iii) one neuron in spiking regime and one in regular bursting regime, both neurons with the same frequencies.

Table 6.1. A list of parameters in the examined pair of Hindmarsh-Rose neurons

	$w_{\text{slow1,1}}$	$w_{\text{slow2,1}}$	w_{fast1}	I_1	$w_{\text{slow1,2}}$	$w_{\text{slow2,2}}$	w_{fast2}	I_2
regular bursting	0.0015	0.019	1.1	3.0	0.0018	0.0012	0.9	2.9
chaotic bursting	0.0050	0.0010	1.1	3.1	0.0022	0.0007	0.9	3.1
one bursting, one spiking	0.0015	0.0009	1.0	5.0	0.0015	0.0009	1.0	2.5

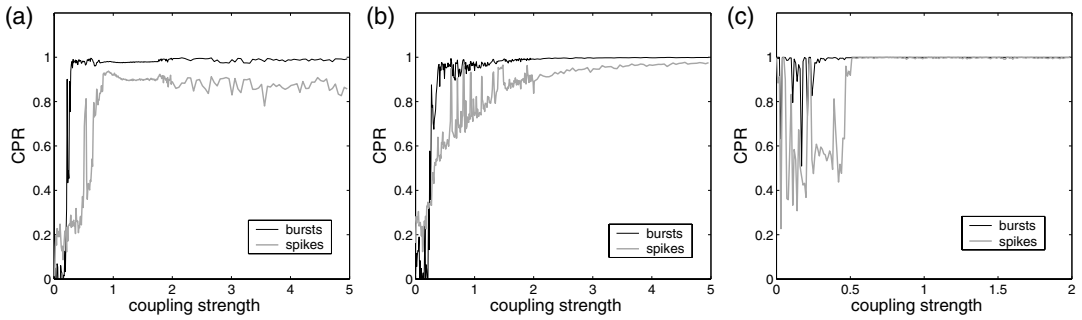

Fig. 6.9. $\text{CPR}^{\text{bursts}}$ and $\text{CPR}^{\text{spikes}}$ vs. coupling strength μ for a pair of Hindmarsh-Rose neurons with parameters according to Table 6.1: (**a**) regular bursting (**b**) chaotic bursting; (**c**) one spiking, one regular bursting

Then, we compute the synchronisation indices $\text{CPR}^{\text{bursts}}$ and $\text{CPR}^{\text{spikes}}$ for each case dependent on the coupling strength (see Fig. 6.9). For all three cases the spikes need higher coupling strengths to become phase synchronized than the bursts. This result is in good accordance with [21].

6.3.2 Analysis of Networks of Neurons

Different network topologies (random, small-world and scale-free) with Hindmarsh-Rose neurons at each node have been analyzed. Each network had $N = 200$ nodes and an average degree $\langle d \rangle$ of 10. The parameters of the neurons have been chosen as follows: $I_n \in \mathcal{N}(3.1, 0.05)$ (chaotic bursting regime), $\omega_{\text{fast},n} \in \mathcal{N}(1, 0.05)$, $\omega_{\text{slow1},n} \in \mathcal{N}(0.002, 0.0005)$, and $\omega_{\text{slow},n} = 0.001$, where $\mathcal{N}(\tilde{\mu}, \sigma)$ denotes a Gaussian normal distribution with mean $\tilde{\mu}$ and variance σ. The coupling strength has been chosen as $\mu = g/\langle d \rangle$. The synchronization indices $\text{CPR}^{\text{bursts}}$ and $\text{CPR}^{\text{spikes}}$ have been calculated for each pair of nodes from the networks for increasing values of the coupling parameter g. Thus, we obtain two matrices $(\text{CPR}^{\text{bursts}}_{\text{nm}})$ and $(\text{CPR}^{\text{spikes}}_{\text{nm}})$, where $n, m = 1, \ldots, 200$ indicate the nodes.

In Fig. 6.10, we present a few snapshots of those CPR-matrices for different values of the coupling strength g for the scale free network. We have found that with an increasing coupling strength, the hubs (nodes with largest degree, see Chap. 3 for details) will synchronize first, while the rest of the nodes need a higher coupling strength to become synchronized. This is in good accordance with [22], where this has been shown for a scale free network of

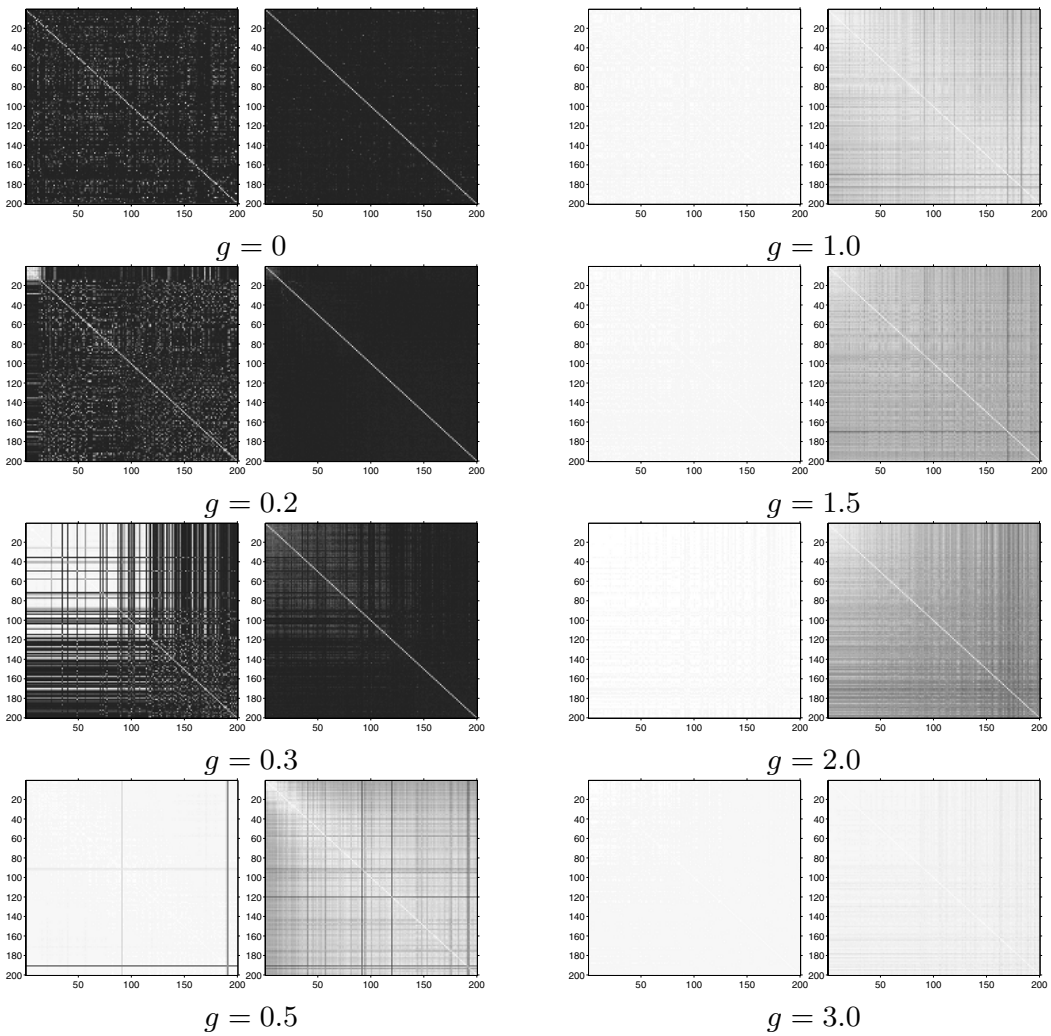

Fig. 6.10. Several snapshots of the CPR matrix of a network of 200 Hindmarsh-Rose neurons are presented for different coupling strengths. The left hand plot of each pair corresponds to the bursts, the right hand one to the spikes, respectively. Several phenomena stand out: 1. the hubs synchronize first, "attracting" the remaining nodes when the coupling increases further; 2. the spikes synchronize for a higher coupling strength than the bursts and; 3. there is a collapse of the spike synchronization in a certain domain of the coupling strength

Rössler oscillators. Furthermore, we have found for all three networks, as in the case of two coupled neurons, that the synchronization of the spikes sets in for higher values of the coupling strength than for the bursts.

To quantify the degree of phase synchronization of the whole network, we count the number of values in (CPR_{nm}) that are above a certain threshold and we call this number "area of synchronization". The threshold has been chosen as 0.8. In Fig. 6.11, those areas of synchronization are plotted versus the coupling strength.

An interesting result can be observed in the plot of the area of synchronization, as well in the snapshots of the CPR-matrices: there is a collapse

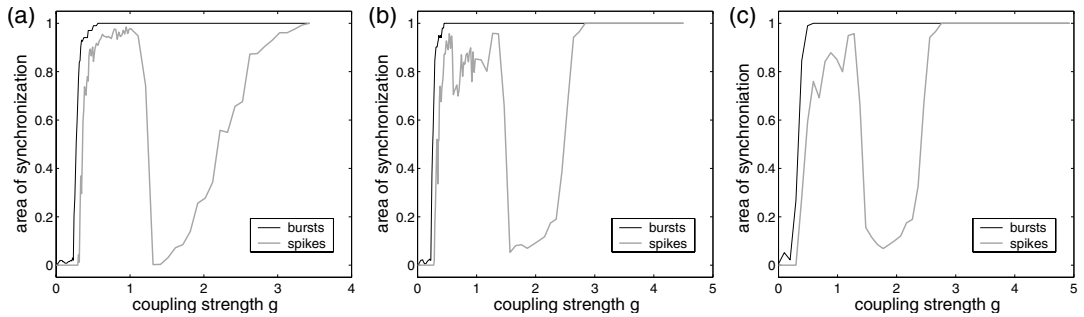

Fig. 6.11. Area of synchronization for; (**a**) random network; (**b**) small-world network; and (**c**) scale-free network for bursts and spikes, respectively

of the synchronization of the spikes for intermediate values of the coupling strength. In contrast, the synchronization of the bursts remains unchanged. This could be due to a change of the dynamics, namely the coherence of the oscillators with increasing values of the coupling strength g.

6.4 Conclusions

In this chapter, we have analyzed phase synchronization in networks with complex topology and complex dynamics. In particular, we have concentrated on dynamics on two time scales, as is typically observed in neurons with spiking and bursting dynamics. In order to analyze the synchronization behavior of such systems we extended an existing method, which is based on the concept of recurrence [11], to treat the two time scales separately. We have applied the proposed method to complex networks of Hindmarsh-Rose neurons. Our results are in accordance with [21], where it has been shown that the spikes need higher values of the coupling strength than the bursts in order to phase synchronize. Moreover, we have found that in a scale-free network of Hindmarsh-Rose neurons, the hubs synchronize first with increasing coupling strength, while the rest of the nodes need a higher coupling to synchronize, as has been reported in [22] for a scale-free network of Rössler oscillators. In addition, the most interesting result of our analysis is that we have found a collapse in the synchronization of the spikes in those complex networks for an intermediate coupling strength. This effect will be discussed in detail in a forthcoming paper.

References

1. S. H. Strogatz, Nature **410**, 268, 2001; M. E. J. Newman, SIAM Rev. **45**, 167, 2003; S. Boccaletti et al., Phys. Rep. **424**, 175, 2006; R. Albert, A.-L. Barabási, *Statistical mechanics of complex networks*, Rev. Mod. Phys., **74**, 47–97, 2002.
2. P. Erdös, and A. Rényi, Publ. Math. Inst. Hung. Acad. Sci. **5**, 17, 1960; D. J. Watts, and S. H. Strogatz, Nature **393**, 440,1998;

L. Barabási, and R. Albert, Science **286**, 509, 1999;
M. Molloy, and B. Reed, Random Struct. Algorithms **6**, 161, 1995.
3. L. Donetti et al., Phys. Rev. Lett. **95**, 188701, 2005.
4. Y. Moreno, and A. F. Pacheco, Europhys. Lett. **68 (4)**, 603, 2004;
J. G. Restrepo et al., Phys. Rev. E **71**, 036151, 2005.
5. F. M. Atay et al., Phys. Rev. Lett. **92 (14)**, 144101, 2004; W. Lu, and T. Chen, Physica D **198**, 148, 2004;
Y. Jiang et al., Phys. Rev. E **68**, 065201(R), 2003.
6. C. Zhou, and J. Kurths, Chaos **16**, 015104 2006.
7. N. F. Rulkov et al., Phys. Rev. E, **51** (2), 980, 1995;
L. Kocarev, and U. Parlitz, Phys. Rev. Lett. **76** (11), 1816, 1996;
S. Boccaletti et al., Phys. Rep. **366**, 1, 2002.
8. B. Blasius et al., Nature **399**, 354, 1999; P. Tass et al., Phys. Rev. Lett. **81 (15)**, 3291, 1998;
M. Rosenblum et al., Phys. Rev. E. **65**, 041909, 2002;
D. J. DeShazer et al., Phys. Rev. Lett. **87 (4)**, 044101, 2001.
9. A. Pikovsky, M. Rosenblum, J. Kurths, *Synchronization - A universal concept in nonlinear science*, Cambridge University Press, 2001.
10. G. V. Osipov, B. Hu, C. Zhou, M. V. Ivanchenko, and J. Kurths, Phys. Rev. Lett. **91**, 024101, 2003.
11. N. Marwan, M. C. Romano, M. Thiel, and J. Kurths, Phys. Rep. **438**, 237, 2007.
12. M. C. Romano, M. Thiel, J. Kurths, I. Z. Kiss, J. L. Hudson, *Detection of synchronization for non-phase-coherent and non-stationary data*, Europhys. Lett., 71 (3), 466, 2005.
13. M. G. Rosenblum, A. S. Pikovsky, J. Kurths, G. V. Osipov, I. Z. Kiss, and J. L. Hudson, Phys. Rev. Lett. **89**, 264102, 2002.
14. C. Sparrow, *The Lorenz equations: Bifurcations, chaos, and strange attractors*, Springer-Verlag, Berlin, 1982.
15. R. N. Madan, *Chua circuit: A paradigm for chaos*, World Scientific, Singapore, 1993.
16. W. Lauterborn, T. Kurz, and M. Wiesenfeldt, *Coherent Optics. Fundamentals and Applications*, Springer-Verlag, Berlin, Heidelberg, New York, 1993.
17. C. L. Weber Jr., and J. P. Zbilut, J. Appl. Physiology **76 (2)** 965, 1994;
N. Marwan, N. Wessel, U. Meyerfeldt, A. Schirdewan, and J. Kurths, Phys. Rev. E **66 (2)**, 026702, 2002;
N. Marwan, and J. Kurths, Phys. Lett. A **302 (5–6)**, 299, 2002; M. Thiel et al., Physica D **171**, 138, 2002.
18. M. Thiel, M. C. Romano, P. Read, J. Kurths, *Estimation of dynamical invariants without embedding by recurrence plots*, Chaos, **14** (2), 234–243, 2004.
19. J. L. Hindmarsh, R. M. Rose, *A model of neuronal bursting using three coupled first order differential equations*, Proc. Roy. Soc. Lond. B **221**, 87–102, 1984.
20. R. D. Pinto, P. Varona, A. R. Volkovskii, A. Szücs, H. D. I. Abarbanel, M. I. Rabinovich *Synchronous behavior of two coupled electronic neurons*, Phys. Rev. Lett. E **62**, nr. 2, 2000.
21. M. Dhamala, V. K. Jirsa, M. Ding *Transitions to synchrony in coupled bursting neurons*, Phys. Rev. Lett. **92**, nr. 2, p. 028101, 2004.
22. C. Zhou, J. Kurths, *Hierarchical synchronization in complex networks with heterogenous degrees* Chaos **16**, 015104, 2006.

A.2 Continuous wavelet transform in the analysis of burst synchronization in a coupled laser system

The article *Continuous wavelet transform in the analysis of burst synchronization in a coupled laser system* has been published in Physical Review E, issue 78, pages 016211, in 2008. I acknowledge the rights for republication within my thesis.

Continuous wavelet transform in the analysis of burst synchronization in a coupled laser system

A. Bergner[1], R. Meucci[2], K.Al Naimee[2,3], M. C. Romano[4],
M. Thiel[4], J. Kurths[1] and F. T. Arecchi[2,5]
[1] *Institute of Physics, University of Potsdam, Potsdam, 14415, Germany*
[2] *CNR-Istituto Nazionale di Ottica Applicata, Largo E. Fermi 6, 50125 Firenze, Italy*
[3] *Department of Physics, University of Baghdad, Baghdad, Iraq*
[4] *College of Physical Sciences, Kings College, University of Aberdeen, Aberdeen AB24 3UE, United Kingdom*
[5] *Department of Physics, Università di Firenze, Firenze, Italy*
(Dated: August 17, 2011)

The transition to synchronization of a pair of coupled chaotic CO_2 lasers is investigated numerically in a model system. This system displays episodes of bursting of different predominant frequencies. Due to the multiple time scales present in this system, we use a complex continuous wavelet transform to perform the synchronization analysis. Thus it enables us to resolve the time of occurrence as well as the frequency of an event in a given time series up to an intrinsic uncertainty. Furthermore, due to the complex nature of that wavelet transform, it yields a direct estimate of the system's phase. We show that, as the coupling strength of the laser system is increased, the mutual coherency increases differently for different frequencies. Additionally we test our method with experimental data.

PACS numbers: 05.45.Pq, 05.45.Tp, 05.45.Xt, 42.65.Pc
Keywords: bursting, multi-time scale, wavelet transform, synchronization

I. INTRODUCTION

Chaotic synchronization is of fundamental importance in a variety of complex systems [1–3]. Synchronization is often studied in autonomous chaotic systems, that is, systems not subjected to an external driving. In this situation, a coupling between two or more systems (identical or not) can induce changes in some properties of the dynamics of the systems, leading to a common behavior.

Here, we consider the case of synchronization of coupled non-autonomous systems, where chaos is due to an external periodic forcing. In particular, we consider bursting chaotic dynamics originated as a consequence of an interior crisis [4, 5]. In contrast to a generic chaotic system, where the attractor is filled almost uniformly in course of time, in a bursting chaotic dynamics there are rather long time intervals spent around unstable periodic orbits (UPOs) laying inside the basin of attraction of the chaotic attractor before the crisis. The time intervals during which the chaotic orbit is attracted by one of these UPOs lead to bursts of high amplitude, which have the predominant period of the corresponding UPO. Thus, a peculiar feature of a bursting chaotic system are such local structures.

As we couple two such bursting chaotic systems, these local structures can be synchronized. For low values of the coupling strength, they become partially synchronized, and as we increase the coupling strength, they become completely synchronized. In this paper we investigate a model system of two coupled CO_2 lasers, and focus on the role of the different time scales present in the system. For this purpose we utilise a complex continuous wavelet transform to resolve different local structures of this multi-time scale system.

The paper is organized as follows. In Sec. II the laser model is presented and the analysis tools are introduced. In Sec. III the results of our analysis are described and in Sec. IV we draw the conclusions.

II. MODEL AND ANALYSIS METHODS

A. The laser model

The model describes a setup of two identical lasers with a common sinusoidal forcing and unidirectional coupling (master-slave coupling). From an experimental point of view such a configuration can be implemented by a single laser whose dynamical regime is controlled via an adequate function generator. Specifically, a master signal is obtained by recording a long time sequence of the laser in a condition where it displays chaotic bursts. In a second stage, the recorded master signal is reproduced by the function generator. The difference signal between the master and the slave laser intensity, amplified by a coupling factor ϵ, is used as an amplitude modulation applied to the sinusoidal driving of the slave laser. This coupling scheme is fairly general allowing coupling between two lasers with nearly identical parameters. The chaotic and synchronization behavior can be reproduced by using the following model of five differential equations for each of the two lasers:

$$\begin{aligned}
\dot{x}_1 &= kx_1(x_2 - [1 + \alpha \sin^2(F_x + B)]), \\
\dot{x}_2 &= -\Gamma_1 x_2 + \gamma x_3 + x_4 + p - 2kx_1x_2, \\
\dot{x}_3 &= -\Gamma_1 x_3 + \gamma x_2 + x_5 + p, \\
\dot{x}_4 &= -\Gamma_2 x_4 + \gamma x_5 + z(x_2 + p), \\
\dot{x}_5 &= -\Gamma_2 x_5 + \gamma x_4 + z(x_3 + p),
\end{aligned} \tag{1}$$

where x represents the slave laser and an identical set of equations exists for the master laser y. The coupling and forcing functions are given by

$$\begin{aligned} F_x &= A\,[1+\epsilon(y_1-x_1)]\sin(2\pi f t), \\ F_y &= A\sin(2\pi f t). \end{aligned} \tag{2}$$

In the above equations, x_1 represents the laser output intensity, x_2 is the population inversion between the two resonant levels, and x_3, x_4 and x_5 account for molecular exchanges between the two levels, resonant with the radiation field and other rotational levels of the same vibrational band. The parameters of the model are the following: $k = 30$ is the unperturbed cavity loss parameter, $\gamma = 0.05$ is a coupling constant, $\Gamma_1 = 10.0643$ and $\Gamma_2 = 1.0643$ are population relaxation rates, $z = 10$ accounts for an effective number of rotational levels, $\alpha = 4$ accounts for the efficiency of the electrooptic modulator, $B = 0.1794$ is a bias voltage, and $p = 0.01987$ is the pump rate. The rest of the parameters are related to the external forcing: the frequency $f = 1/7$ and the amplitude $A = 0.1044$, which are set to a value where the system exhibits chaotic bursting, ϵ is the master-slave coupling strenght. For more details on the model see [7–9].

If the system is uncoupled and autonomous ($A = 0$) the subsystems show a fixed point dynamics. When the external forcing is introduced ($A > 0$) but without coupling ($\epsilon = 0$), the lasers are in a self sustained regime and show tonic spiking with the frequency f of the periodic forcing (an exemplary time series for each laser is shown in Fig. 1). The spike occurrences of both subsystems are locked perfectly due to their common forcing, however, considering that the initial conditions are different, the spike amplitudes of both systems are uncorrelated. This is the typical behavior of systems which are phase synchronized due to a common driving signal [2, 3]. On a larger time scale, it becomes visible that bursts of higher amplitude – i.e. groups of consecutive spikes with high amplitude – occur repeatedly but irregularly (see time series in Fig. 4 (a)). The creation of these bursts can be explained as follows.

By increasing the amplitude A of the sinusoidal driving, the laser undergoes a sequence of subharmonic bifurcations leading to a small amplitude chaotic attractor. A further increase of A leads to an interior crisis [4, 5, 10], whereby the chaotic attractor suddenly expands, including phase space regions of other unstable orbits. Shortly after the crisis, an intermittent regime (crisis-induced intermittency) is established where bursts of high amplitude orbits of period three and four are intercalated with the chaotic attractor before the crisis. The bursting regime investigated here is not a bistable regime. Bistability in this model occurs for lower values of the parameter A (the amplitude of the intrinsic modulation) [11], but we do not consider this regime here.

By introducing the coupling into the system ($\epsilon > 0$) we can synchronize both lasers. The synchronization studied here is not the one of the spikes, which are, as already mentioned, locked perfectly, but the synchronization of the bursts, or to be more precise the synchronization of the UPOs of different length. In the numerical system we only observe in-phase synchronization of those orbits, however, in the time series recorded from the experiment we also observe anti-phase sychronization during the high amplitude bursts [9].

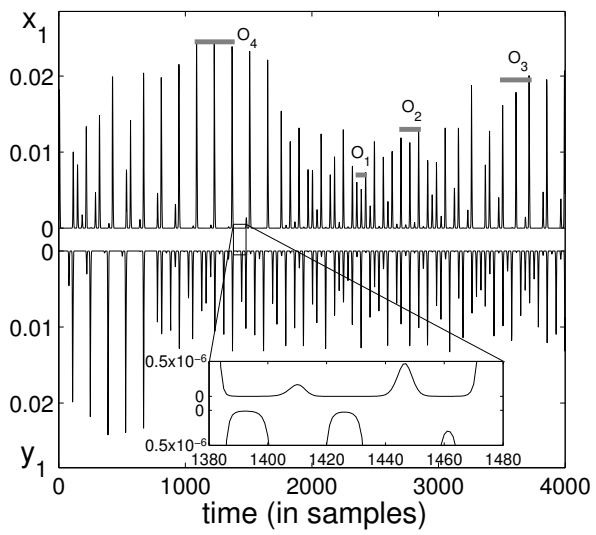

FIG. 1: Time series of the laser intensities x_1 and y_1 from the model system (1) in the uncoupled mode ($\epsilon = 0$). The portion of the time series, displayed in the zoomed box, demonstrates that there is a spike on every period of the forcing frequency f. Time durations of local structures are denoted by O_i segments; precisely, O_1, O_2, O_3, and O_4 denote intervals during which the trajectory passes close to an UPO of period 1, 2, 3, 4, respectively. See text and Fig. 2 for more details.

Due to the strong periodic forcing (2), the rotation times of all orbits are locked to integer factors of the frequency f of the forcing. A spike is created after a full rotation of the trajectory across the attractor. An exhibition of trajectories passing nearby different periodic orbits that exist inside the attractor is presented in Fig. 2. We find segments of orbits, which can have cycling times one to four times the forcing period. Larger spikes (larger values of x_1) are created by orbits with longer periods.

The orbits of different length create the different time scales present in this system, i.e., a multi-time scale system is generated. A coupling between both laser systems might lead to a synchronization on these different time scales between both systems. With an adjustment of the coupling strength ϵ, the visitings of the UPOs may occur simultaneously in both subsystems, which manifests in a synchronization of the bursts of both lasers. Due to the multiple time scales in this system, which arise from the different UPOs present in the attractor, a continuous wavelet transform represents an appropriate tool for a synchronization analysis.

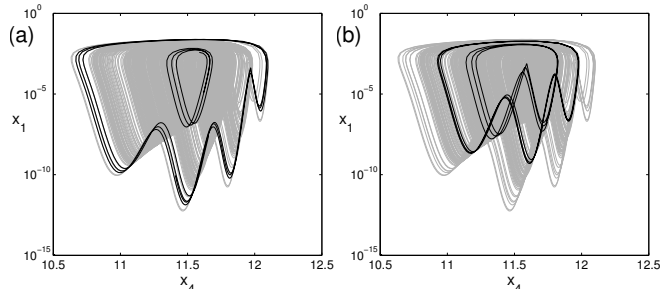

FIG. 2: x_1-x_4-projection of the laser's attractor plotted together with trajectories passing nearby unstable periodic orbits of different length. (a) orbits of length 1 and 4, and (b) orbits of length 2 and 3.

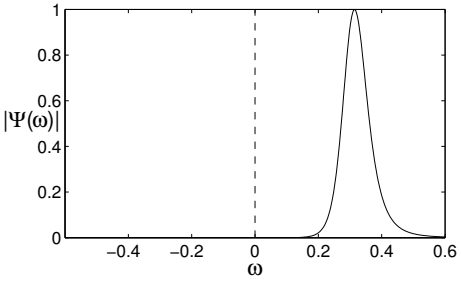

FIG. 3: The magnitude of the Fourier transform $\Psi(\omega)$ of the wavelet (4) for $p = 0.75$. Note, that the negative frequencies are basically zero, which gives the wavelet its nice analytic properties.

B. Continous wavelet transform

The continuous wavelet transform (CWT) has been developed to resolve events localized in time as well as in frequency. It can be interpreted as a constant Q bandpass filterbank (Q = bandwidth/center-frequency = const). In mathematical terms the CWT $\mathcal{W}_\psi x$ of a function $x(t)$ is defined as

$$\mathcal{W}_\psi x\,(\sigma,\tau) \;:=\; \frac{1}{\sigma}\int_{\mathbb{R}} \psi^*\!\left(\tfrac{t-\tau}{\sigma}\right)\, x(t)\; dt \qquad (3)$$

with the mother wavelet $\psi(t)$ translated by τ and dilated by σ. The raised star denotes complex conjugation. The choice of the mother wavelet ψ is mainly influencing the time-scale-uncertainty of the resulting wavelet transform. For more background on the CWT see for example [12].

The numerical computation of the wavelet transform in this work is performed by using systems of linear difference equations. This approximate method to calculate the CWT has the advantage of a very short computation time which is also independent of the wavelet's scale. The wavelet used here is given by its z-transform

$$\mathcal{Z}\psi \;=\; \Psi(z) \;=\; H(z)\; H^*(1/z^*) \qquad (4)$$

with

$$H(z) \;=\; \frac{1}{4}\left(\frac{1-p}{z-ip}\right)^3 (z^2-1)(z-i), \qquad (5)$$

where $H(z)$ is the systems transfer function and $p \in [0,1]$ is a parameter which allows to smoothly alter the degree of localization of the wavelet in either time or frequency. However, this method has the drawback that the transformed signal is not completely analytic, and that the wavelet changes its shape slightly under the rescaling process. Nevertheless, if p is choosen high enough ($p > 0.6$), these problems can be neglected. Figure 3 displays the magnitude of the Fourier transform $\Psi(\mathrm{e}^{\mathrm{i}\omega})$ of this wavelet for $p = 0.75$, which is the value that has been used in our analysis. This wavelet can be compared with the Cauchy-Paul-Wavelet. A detailed explanation of this wavelet will be given in a forthcoming paper [13].

The complex valued CWT has the advantage over the real valued CWT that it can be immediately split into a phase and an amplitude at each point (σ,τ). Thus the existing methods for detecting phase synchronization can be applied very easily.

C. Measuring synchronization and coherency

Phase synchronization (PS) is characterized by the adaptation of the typical time scales between two systems, while their amplitudes may stay nearly uncorrelated. If one deals with narrow-band oscillatory dynamics, also called phase coherent, simple phase definitions exist, e.g., based on the rotation of the trajectory or based on the Hilbert transform [3, 6], that yield good results (see also [14] for a comparison). However, in case of non-phase-coherent dynamics, such as multiple time scales, other approaches are necessary. So far techniques basing on special filters [15], on curvature [16], or on recurrence [17, 18] have been proposed. Also in the case of different time scales being present in the system, there is no general method to define the phase of the system. A complex CWT is advantageous for this purpose, because due to its complex nature, it yields a direct estimate of the phase for each time scale of the system. In order to quantify PS, we use two different measures, namely, the mean resultant length (also known as vector strength) and the cross correlation coefficient combined with a complex CWT.

The mean resultant length is defined as follows

$$r_{xy} \;:=\; \left|\langle e^{i\Delta\phi_{xy}(t)}\rangle\right| \;=\; \left|\frac{1}{T}\sum_{t=1}^{T} e^{i\Delta\phi_{xy}(t)}\right|, \qquad (6)$$

where $\Delta\phi_{xy}(t) := \phi_x(t) - \phi_y(t)$ denotes the phase difference between both systems at time t. We extract the phases $\phi_{x,y}(t)$ directly from the argument of the CWT: $\phi_x(t) = \arg \mathcal{W}_\psi x_1(\sigma,t)$, and analogously for y_1. The mean resultant length r_{xy} can assume values from 0 to 1 and quantifies the strength of the mean angle of the circularly distributed values (here the phase differences

$\Delta\phi_{xy}$). If $r_{xy} = 0$, it indicates that all values of $\Delta\phi_{xy}$ are equally distributed over the interval $[0, 2\pi)$, indicating that there is no synchrony between the phases ϕ_x and ϕ_y. The value $r_{xy} = 1$ indicates that all phase differences are equal and thus the phase differences are locked perfectly at all times. Since the phases of chaotic systems usually show a certain amount of phase diffusion, one expects values less than 1, but still considerably larger than 0, if their phases are synchronized. Note, that the mean resultant length is similar to the Kuramoto parameter [2, 19], but with mean over time instead of being computed over an ensemble of oscillators.

The cross correlation coefficient (CCC) is a linear measure for the similarity between two signals and is given by

$$\rho_{xy} := \frac{\langle xy^* \rangle}{\sqrt{\langle |x|^2 \rangle \langle |y|^2 \rangle}}, \tag{7}$$

where $\langle . \rangle$ denotes the mean over time and the signals x and y are considered to be mean free. This is the case here, since it is a property of the CWT to remove the mean from signals. In general ρ_{xy} can be complex valued (in the case of analytic signals) with an arbitrary angle and a modulus between 0 and 1. A modulus of 0 means that there is no linear correlation between the signals, and a value of 1 indicates that the signals are completely linearly correlated, thus differ only by a factor. The modulus of the complex CCC is also known as coherence.

As Eq. (7) is the normalized scalar product of x and y, thus, the CCC measures the orthogonality between two functions. Since we have that $\langle \sin \omega_1 t, \sin \omega_2 t \rangle = \delta_{\omega_1 \omega_2}$ (where δ_{nm} denotes the Dirac delta) and that PS also implies a coincidence of the frequencies, it is clear that the CCC can be used to detect PS. However, in the case of two real, oscillatory signals the coefficient's modulus fluctuates arbitrarily between 0 and 1 if the phase differences of the two signals are altered. In the extreme case we have $\langle \sin \omega t, \cos \omega t \rangle = 0$, even though intuitively they should be considered to be phase synchronized. In that case one has to calculate the cross correlation function and search the appropriate delay (in the sine-cosine case it is $\pi/2$). This requires much more computations compared to the calculation of the mere CCC, which is the cross correlation function at delay zero.

The complex wavelet used here yields an analytic signal. For analytic signals the phase delay between two signals of equal frequency plays no role, since it can be factored out: $\langle e^{i(\omega t+\phi)}, e^{i\omega t} \rangle = e^{i\phi} \langle e^{i\omega t}, e^{i\omega t} \rangle = e^{i\phi}$. Thus, for analytic signals the CCC is stable under phase shifts and can be used as a measure for PS.

III. RESULTS AND DISCUSSION

Before applying the measures for synchrony and coherency, one needs to consider what the wavelet spectrum reveals and how it can be used together with the above measures to get more insights into the synchronization behavior of the system.

A. Interpretation of the wavelet spectrum

The data has been logarithmized before the computation of the CWT in order to transform the exponentially shaped spikes into a more sinusoidal-like shape (see time series in Fig. 5 in comparison to the time series in Fig. 1). Thus the resulting wavelet spectrum looks cleaner, since it contains less higher harmonic components. Fig. 4 shows an exemplary (original) time series and the corresponding CWT of the logarithmized data.

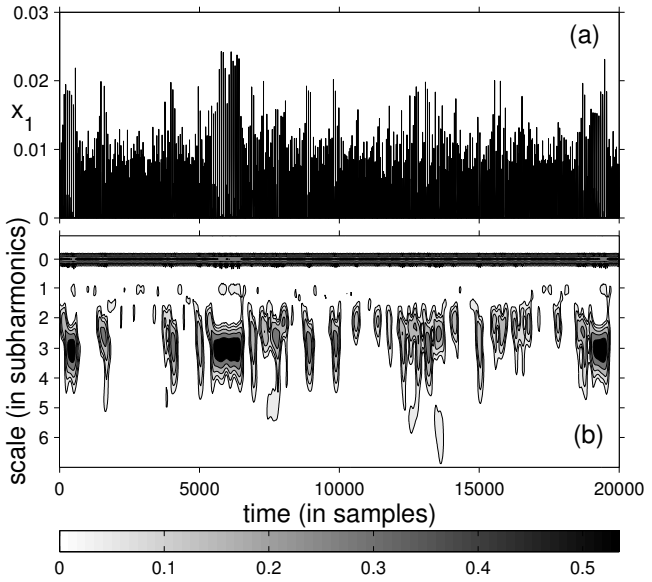

FIG. 4: A time series of the x_1 component of the model system (1), (2) (a) and the corresponding wavelet power spectrum (b) of the logarithmed data. The spiking frequency f of the laser has been normalized to be scale 0, so that the subharmonics are numbered with 1,2,3,... for the first, second, third, and so on subharmoinc, respectivly.

The continuous horizontal line (normalized to be scale 0) in the CWT of the numerically integrated laser model corresponds to the system's intrinsic spiking frequency f which is caused by the periodic forcing. On larger scales patches occur at those times where we find bursts in the time series. This can be understood as follows. As we explained in section II, bursts in the time series are created by trajectories passing nearby UPOs with cycling times that are multiples of the forcing's frequency (see again Fig. 2). Hereby subharmonics of that frequency are created which will become visible as patches at the corresponding scale in the wavelet power spectrum (see Fig. 4 and also Fig. 5 for a magnification of a burst).

Hence, the CWT of the laser model data allows quantifying easily synchronization between the different time

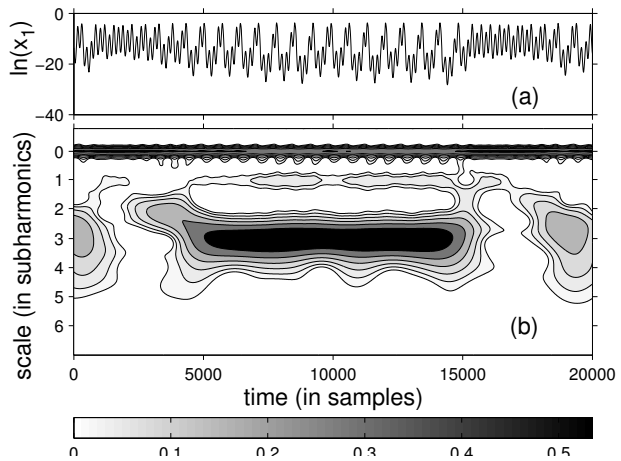

FIG. 5: Magnification of the large burst after sample 5000 in Fig. 4, here with the logarithmed time series in (a). This is a local structure created by the influence of a period four orbit, which becomes visible in the CWT as a third subharmonic.

scales and yields a method to indirectly study the synchronization characteristics of the individual periodic orbits.

Figure 6 shows the CWT for a time series recorded from the experiment. The laser intensity signal has been recorded at the onset of the bursting behavior for an amplitude value $A = 0.108$ (such a value is about 3% different from the numerical value). Note, that computing the logarithm of the data does not reduce the higher harmonics in the same amount as in the numerical case. The wavelet power spectrum displays higher harmonics of the subharmonics, which appear as patches around scale 0.5.

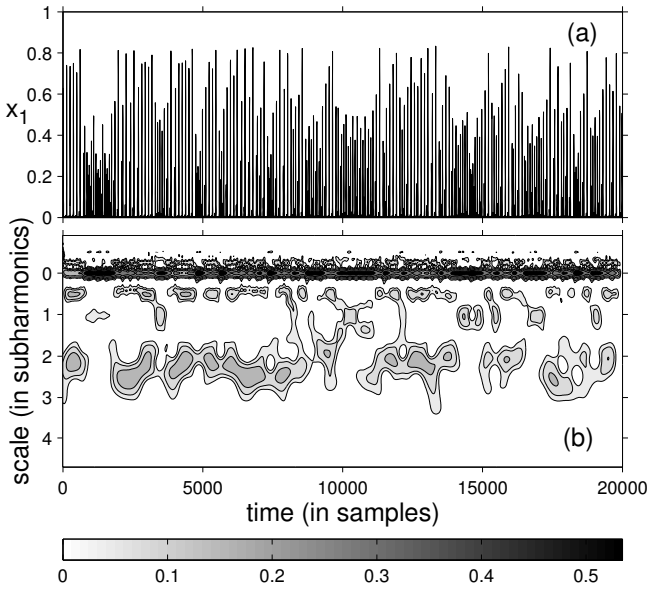

FIG. 6: Same as Fig. 4, but here for experimental data. See text for more details.

B. Multiscale synchronization analysis

We combine now the methods of section II to perform a multiscale synchronization analysis. We calculate (6) and (7) for different values of the coupling strength ϵ and for each scale σ of $\mathcal{W}_\psi x_1$ and $\mathcal{W}_\psi y_1$ of the laser intensities from the model system (1) and from experimentally recorded data.

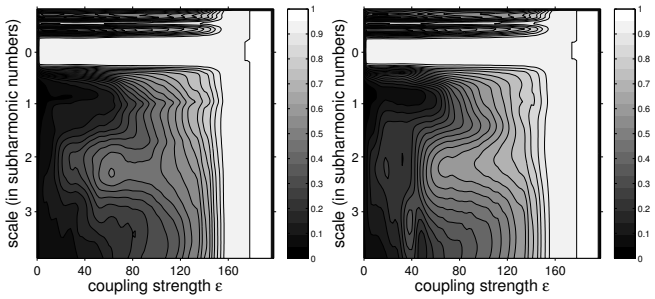

FIG. 7: The results of the multi-scale synchronization analysis for the model system (1). Left: the mean resultant length $r(\sigma, \epsilon)$, and right: the modulus $|\rho(\sigma, \epsilon)|$ of the cross correlation coefficient.

For the model system the measures were calculated for values of ϵ from 0 to 200. The resulting functions $r(\sigma, \epsilon)$ and $|\rho(\sigma, \epsilon)|$ are shown in Fig. 7. Qualitatively, both measures yield similiar results. At $\epsilon \approx 160$, both systems become almost completely synchronized, as it has been already reported in [9]. But here we see in detail that there is almost complete synchronization on all scales.

The new result obtained from our analysis is the observation of a diverse transition to synchronization of the coupled model system on its different time scales. In particular we see an increase of phase coherency among the period three orbits (second subharmonics) between both subsystems for relatively low values of the coupling strength ϵ, whereas the coherency between the other orbits (period two and four) starts increasing for much higher values of ϵ. This result is obtained with both, the mean resultant length and the correlation coefficient.

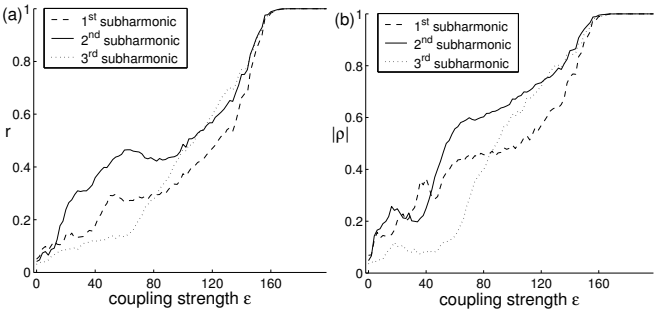

FIG. 8: The measures of synchronization for the model system (1) plotted only for the three subharmonics ($\sigma = 1, 2, 3$). (a) mean resultant length $r(\epsilon)$, (b) modulus $|\rho(\epsilon)|$ of the cross correlation coefficient.

Figure 8 shows $r(\epsilon)$ and $|\rho(\epsilon)|$ only for the three subharmonics. Here one can follow the transition to full synchronization for each of that three time scales. Especially for coupling strength bewteen 40 and 80 the difference in the amount of synchrony of the subsystems beween the 2nd and the 3rd subharmonic is rather strong.

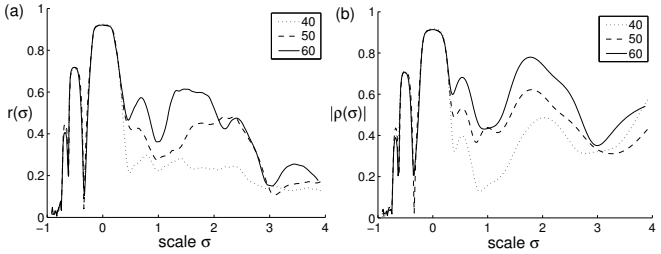

FIG. 9: Results from experimental measurements. (a) The mean resultant length $r(\sigma)$, (b) the modulus $|\rho(\sigma)|$ of the correlation coefficient. The coupling strengths are 40, 50, and 60, respectively.

In the analysis of experimental data, collected using the master-slave experimental setup described at the beginning of Sec. II, we used three different values of the coupling strength ϵ. Figure 9 shows again both measures of sychronization but here plotted against scale. Both measures reveal clearly an increase of synchronization between the second subharmonics of both lasers as the coupling strength is increased. Note, that the maxima at $\sigma \approx 0.5$ result from the higher harmonics which have already be discussed in Sec. III A. Further, note that the maxima of the curves are not aligned for the different coupling strengths. This is caused by the fact that we used much less data for the calculation of the presented figures compared to the numerical case. Therefore transients in which the systems is between two orbits and which appear between the subharmonic scales in the CWT have a much larger impact in the statistical analysis. A more detailed discussion of the experiment will be presented elsewhere.

IV. CONCLUSIONS

We have numerically studied the synchronization of bursts in a model system of two externally forced coupled CO_2 lasers with master-slave coupling. The bursts in this system have different predominant frequencies, which arise from unstable periodic orbits of different lengths embedded in the chaotic attractor.

For multi-time scale systems no standard measures for phase synchronization exist. Therefore we have applied a complex continous wavelet transform to the data of the lasers' intensities in order to decompose the multiple time scales of that system. We have combined this approach with two measures for phase synchronization, namely, the mean resultant length and the cross correlation coefficient. This procedure enables us to identify details of synchronization of these multi-time scale systems. In particular, we have found that as we increase the coupling strength, there is an early increase of synchronization between periodic orbits of period three, where the fundamental period is given by the period of the forcing. This new insight was not known from previous analysis, carried out with standard methods. This multiple time scale synchronization analysis has also been tested with experimental data, where we have found qualitatively the same results.

The analysis method presented in this paper can be extended to apply to a general class of multi-time scale systems, such as neuronal dynamics, where spiking and bursting play a key role in the communication among neurons [20, 21].

Acknowledgements

A. Bergner acknowledges financial support from the International Max Planck Research School on Biomimetic Systems. A. Bergner, R. Meucci and J. Kurths acknowledge financial supportfrom COST B27 Electric Neuronal Oscillations and Cognition. K.Al Naimee acknowledges Landau Network - Centro Volta, Como for financial support. M.C. Romano acknowledges the Scottish Universities Life Sciences Alliance (SULSA) for financial support. M. Thiel acknowledges RCUK for financial support.

[1] L. M. Pecora, T. L. Carroll, *Synchronization in chaotic systems*, Phys. Rev. Lett. **64**, pp. 821-824, 1990.
[2] A. Pikovsky, M. Rosenblum, J. Kurths, *Synchronization - A universal concept in nonlinear science*, Cambridge University Press, 2001.
[3] S. Boccaletti, J. Kurths, G. Osipov, D. L. Valladares, C. Zhou, *The synchronization of chaotic systems*, Physics Reports **366**, pp. 1-101, 2002.
[4] C. Grebogi, E. Ott, and J. A. Yorke, Phys. Rev. Lett. **48**, 1507, 1982.
[5] C. Grebogi, E. Ott, and J. A. Yorke, Physica D **7**, 181, 1983.
[6] M. Rosenblum, A. Pikovsky, J. Kurths, *Phase Synchronization of Chaotic Oscillators*, Phys. Rev. Lett. E, vol. 76, nr. 11, pp. 1804-1807, 1996.
[7] A. N. Pisarchik, R. Meucci, F. T. Arecchi, *Theoretical and experimental study of discrete behavior of Shilnikov chaos in a CO_2 laser*, Eur. Phys. J. D **13**, pp. 385-391,

2001.

[8] R. Meucci, D. Cinotti, E. Allaria, L. Billings, I. Triandaf, D. Morgan, I. B. Schwartz, *Global manifold control in a driven laser: sustaining chaos and regular dynamics*, Physica D **189**, pp. 70-80, 2006.

[9] R. Meucci, F. Salvadori, M. V. Ivanchenko, K. Al Naimee, C. Zhou, F. T. Arecchi, S. Boccaletti, J. Kurths, *Synchronization of spontaneous bursting in a CO_2 laser*, Phys. Rev. E **74**, 066207, 2006.

[10] C. Grebogi, E. Ott, F. Romeiras, and J. A. Yorke, Phys. Rev. A **36**, 5365, 1987.

[11] R. Meucci, E. Allaria, F. Salvadori, F. T. Arecchi, *Attractor Selection in Chaotic Dynamics*, Phys. Rev. Lett. **95**, 184101, 2005.

[12] M. Holschneider, *Wavelets: an analysis tool*, Oxford University Press, 1995.

[13] A. Bergner, J. Kurths, *Fast approximation of complex continous wavelet transform with recursive IIR filters*, in preperation.

[14] T. Pereira, M. S. Baptista, J. Kurths, *Phase and average period of chaotic oscillators*, Phys. Lett. A **362**, pp. 159-165, 2007.

[15] M. Rosenblum, A. Pikovsky, J. Kurths, *Locking-Based Frequency Measurement and Synchronization of Chaotic Oscillators with Complex Dynamics*, Phys. Rev. Lett. **76**, 26, p. 264102, 2002.

[16] G. V. Osipov, B. Hu, C. Zhou, M. V. Ivanchenko, J. Kurths *Three Types of Transitions to Phase Synchronization in Coupled Chaotic Oscillators*, Phys. Rev. Lett. **91**, 2, pp. 024101, 2003.

[17] M. C. Romano, M. Thiel, J. Kurths, I. Z. Kiss, J. L. Hudson, *Detection of synchronization for non-phase-coherent and non-stationary data*, Europhys. Lett. **71**, 3, pp. 466, 2005.

[18] N. Marwan, M. C. Romano, M. Thiel, J. Kurths, *Recurrence plots for the analysis of complex systems*, Physics Reports **438**, pp. 237-329, 2007.

[19] Y. Kuramoto, *Chemical Oscillations, Waves, and Turbulence*, Springer-Verlag Berlin Heidelberg, 1984.

[20] J. E. Lisman, *Bursts as a unit of neural information: making unreliable synapses reliable*, Trends Neurosc. **20**, issue 1, pp. 38-43, 1997.

[21] E. M. Izhikevich, N. S. Desai, E. C. Walcott, F. C. Hoppensteadt, *Bursts as a unit of neural information: selective communication via resonance*, Trends Neurosc. **26**, issue 3, pp. 161-167, 2003.

A.3 Remote Synchronization in Complex Networks

The article *Remote Synchronization in Complex Networks* is at the time of publication of this thesis not yet published as it is still in the referee process. It will most likely be published in Physical Review E at the end of 2011. I acknowledge the rights for prepublication within my thesis.

Remote Synchronization in Complex Network

A. Bergner[1,3], M. Frasca[2], G. Sciuto[2], A. Buscarino [2], E.J. Ngamga[3], L. Fortuna[2], J. Kurths[3,4]
[1] *Institute of Physics, University of Potsdam, 14476 Potsdam, Germany*
[2] *DIEEI, Faculty of Engineering, University of Catania, 95125 Catania, Italy*
[3] *Potsdam Institute for Climate Impact Research (PIK), 14473 Potsdam, Germany*
[4] *Institute of Physics, Humboldt University, Berlin, Germany*
(Dated: August 13, 2011)

We study phase synchronization (PS) in a network motif with a star-like structure in which the central node's (the hub) frequency is strongly detuned against the other peripheral nodes. We find numerically and experimentally a regime of remote synchronization (RS), where the peripheral nodes form a phase synchronized cluster, while the hub remains free with its own dynamics and serves just as a transmitter for the other nodes. We explain the mechanism for this RS by the existence of a free amplitude and also show that systems with a fixed or constant amplitude, such as the classic Kuramoto phase oscillator, are not able to generate this phenomenon. Further we derive an analytic expression which supports our explanation of the mechanism.

PACS numbers: 05.45.Xt, 89.75.Hc, 89.75.-k, 89.20.Kk
Keywords: synchronization, networks

I. INTRODUCTION

Networks of oscillatory units have been recently studied widely [1–4]. These kinds of systems serve as a modeling basis for a variety of systems from neuroscience [5], pattern recognition [6], chemistry [7], biology [8], climatology [9–11], ecology [12], social systems [13], or engineering as for instance in robot coordination [14], communication [15] and sensor networks [16], and as a general concept for understanding complex self-organizing systems. Gaining knowledge about networks of coupled dynamical systems helps understanding several phenomena, in particular synchronization, self-organization and information transfer in complex systems.

Many networks found in nature have a scale-free topology [1, 17], which is a structure where just a few nodes—the so called hubs—hold the major bulk of the links. In this work we study a typical network motif of such a hub [Fig. 1]. It is interesting to study synchronization in such a hub motif as it captures the essence of scale-free topologies.

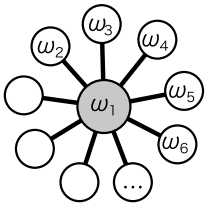

FIG. 1. Graphic visualization of a hub network motif (star motif).

Many articles on oscillatory networks focus on a rather homogenous distribution of the nodes' parameters across the network, i.e. all nodes are either identical or just detuned within a small parameter range. This is very likely due to the possibility of an analytical treatment of the underlying equations, which becomes very complicated or even undoable if the network and thus the describing equations become too heterogenous. But the assumption of homogeneity is, in fact, not fulfilled in most realistic situations, that means it's quite unlikely to find a real system made up of several absolutely identical subsystems.

Therefore, we study in this work an oscillatory network model and focus on a strong heterogeneity, precisely, the frequency of the hub is strongly detuned with respect to the peripheral nodes. We investigate phase synchronization (PS) in these motifs. Within this setup we focus on a phenomenon which we will call *remote synchronization* (RS), that is a situation in which two or more nodes, say n and m, which are not coupled directly, but through other nodes only, are phase synchronized, but, and this is important, the transmitter nodes, i.e. the nodes along the path from n to m are not phase synchronized with n and m, respectively.

We also investigate remote synchronization experimentally. To this aim, we designed a complex network made of coupled electronic nonlinear oscillators and study it with respect to different values of the coupling strength. The experimental results obtained confirm the emergence of remote synchronization in real systems.

In addition to numerical and experimental studies we give necessary conditions for the existence of RS and show that fixed amplitude systems, such as Kuramoto phase oscillators cannot generate the phenomenon, and explain this analytically, as well.

The outline of this paper is the following. First we introduce our model and the parameters and give a description of the experimental setup. Then we describe the observed phenomena and present analysis of them. Finally we discuss the outcome and explain the underlying mechanism.

II. MODEL AND EXPERIMENTAL SETUP

Since we want to focus on the mere phenomenon of synchronization, in particular PS, we chose a simple and paradigmatic model, namely the Stuart-Landau oscillator. This model is the most simple one having a harmonic limit cycle without any distortions, so we can exclude n:m synchronization in our analysis for now.

We consider a network of diffusively coupled Stuart-Landau oscillators [7, 18]. The equations are given by

$$\dot{u}_n = (\alpha + i\omega_n - |u_n|^2)u_n \; + \; \frac{\varkappa}{d_n^{\text{in}}} \sum_{m=1}^{N} g_{nm}(u_m - u_n), \quad (1)$$

where $u \in \mathbb{C}$, α is the (Hopf) bifurcation parameter which controls how fast the trajectory will decay onto the attractor, ω_n is the eigen frequency of the individual uncoupled oscillator n, $\varkappa$ is the overall or global coupling strength, d_n^{in} is the in-degree of node n and is used to normalize the input into node n, and (g_{nm}) is the adjacency matrix, which is symmetric, since we consider bidirectional couplings.

Now we give the values of the parameters used for the simulations in this paper. The number of nodes has been set to $N = 5$ in correspondence with our experimental setup, but we also verified numerically the existence of the phenomenon for higher values of N. The decay parameter is $\alpha = 1$. As mentioned in the introduction we are analyzing a hub motif (star-like network, Fig. 1), due to its importance as building block for scale-free networks. Node 1 is chosen to be the hub and thus $n = 2 \ldots N$ subscripts the peripheral nodes. The adjacency matrix is given by

$$(g_{nm}) = \begin{pmatrix} 0 & 1 & 1 & 1 & 1 \\ 1 & 0 & 0 & 0 & 0 \\ 1 & 0 & 0 & 0 & 0 \\ 1 & 0 & 0 & 0 & 0 \\ 1 & 0 & 0 & 0 & 0 \end{pmatrix}.$$

The in-degrees are $\{d_n^{\text{in}}\} = \{4, 1, 1, 1, 1\}$. We chose the frequency of the hub to be $\omega_1 = 2.5$ in the beginning, but we will discuss the influence of a continuous change of this value later, as well. The peripheral nodes have a similar frequency but not identical, since some repelling force is needed in order to see the transition to PS. The frequencies used in numerical simulations are $\{\omega_n\}_{n=2}^{5} = \{0.975, 0.992, 1.008, 1.025\}$

For the experimental realization Eq. (1) must be transformed into its equivalent real form which is given by

$$\begin{aligned} \frac{d}{dt}\begin{pmatrix} x_n \\ y_n \end{pmatrix} \; = \; & \left[\begin{pmatrix} \alpha & -\omega_n \\ \omega_n & \alpha \end{pmatrix} - (x_n^2 + y_n^2)\mathbb{1} \right] \begin{pmatrix} x_n \\ y_n \end{pmatrix} \\ & + \frac{\varkappa}{d_n^{\text{in}}} \sum_{m=1}^{N} g_{nm} \left[\begin{pmatrix} x_m \\ y_m \end{pmatrix} - \begin{pmatrix} x_n \\ y_n \end{pmatrix} \right]. \end{aligned} \quad (2)$$

The experimental setup is based on an electronic circuit mimicking the behavior of the Stuart-Landau oscillator. The circuit made of discrete components (operational amplifiers, multipliers realizing the nonlinearities of the oscillator, and a number of passive components such as resistors and capacitors) has been designed in order to obey to the same equations [Eq. (2)] of the Stuart-Landau oscillator, after appropriate scaling in frequency. We designed the circuit by following the guidelines reported in [19] and used for instance in [20, 21]. The values of some components of the hub and peripheral circuits are chosen in a different way so that to realize the different simulation parameters used for hub and peripheral nodes. The circuits have been then coupled in such a way that a single resistor for each node controls the value of the coupling strength in Eq. (2). The circuit schematic, the governing equations and the used component values are reported in appendix A.

III. EMERGENCE OF REMOTE SYNCHRONIZATION

We start our analysis with a visual inspection of numerically integrated time series of system (1). Fig. 2 depicts the excerpts from the time series as well as the instantaneous frequencies and Lissajous-like patterns of the phases. For low coupling [Fig. 2(a)] we see that the nodes are interacting with each other and modulations of the phase appear, but no synchronization is visible. For a strong coupling [Fig. 2(c)] we find a regime of full phase synchronization with an identical amplitude of all nodes and without any modulations. The phenomenon of RS appears for intermediate values of the coupling strength [Fig. 2(b)]. Here we see, that all peripheral nodes become phase synchronized, while the hub remains with its own phase and frequency.

In order to study this more precisely, we will introduce some measures for PS. The most common measure for PS is the Kuramoto order parameter, which is defined:

$$r_{nm} = \left| \langle e^{i[\varphi_n(t) - \varphi_m(t)]} \rangle_t \right|, \quad (3)$$

where $\langle . \rangle_t$ denotes the mean over time, and $\varphi_n(t)$ is the phase of oscillator n. For the Stuart-Landau oscillator the phase is simply given by $\varphi(t) = -i \log(u/|u|)$.

Since we are interested in the situation where the peripheral nodes form one synchronized cluster and the hub is separated from this, i.e. it forms another trivial cluster with itself, we introduce two measures accounting for that situation. For measuring the coherence of the hub with the rest of the network we define $r^{\text{direct}} = \frac{1}{N-1} \sum_{n=2}^{N} r_{1n}$. As a measure for the coherence of the peripheral cluster we define $r^{\text{indirect}} = \frac{2}{(N-1)(N-2)} \sum_{n=2, m>n}^{N} r_{nm}$, i.e. the mean of the pairwise measured phase coherence among the peripheral nodes.

Fig. 3 shows the transition to PS of both measures in dependence on the coupling strength $\varkappa$. The measures have been computed from numerical integration of Eq. (1) with the parameter setup given in Sec. II. Here it is

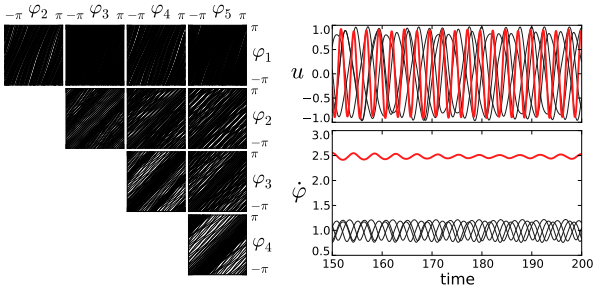

(a) Snapshots for $\varkappa = 0.2$. Here no synchronization between any nodes is visible.

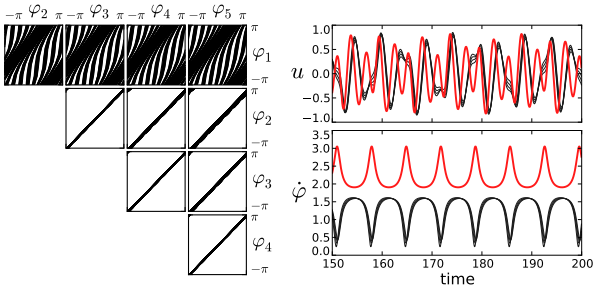

(b) Snapshots for $\varkappa = 0.6$. Here we find remote synchronization. The peripheral nodes are synchronized with each other while the hub (node 1) remains unsynchronized with the rest.

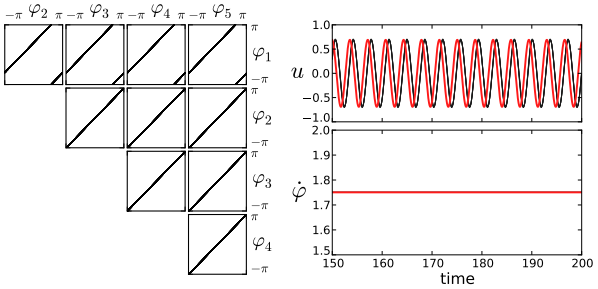

(c) Snapshots for $\varkappa = 0.8$. Regime of full phase synchronization. All nodes of the network are synchronized with each other.

FIG. 2. (Color online) These plots shall help to understand the observed phenomena. For three different values of the coupling strength $\varkappa$ snapshots are shown of: the time series $u(t)$, the instantaneous frequencies $\dot{\varphi}(t)$ and Lissajous-like figures made by plotting pairwise the phases φ_n of all oscillators against each other. The red line is the hub.

clearly visible that the phase coherence of the peripheral nodes increases considerably faster than the synchronization of the hub with the rest. The peripheral nodes reach full PS at a value of the coupling strength $\varkappa$ of about 0.47, while the hub joins this cluster much later at $\varkappa \approx 0.74$, when it hits the global Arnold tongue of the network. In the figure we marked three steps in the curve of r^{indirect}. These steps correspond to the onset of RS between two, three and all (four in our case) peripheral nodes of the network. These transitions are more clearly visible in Fig. 5(b) in which the number of synchronized clusters

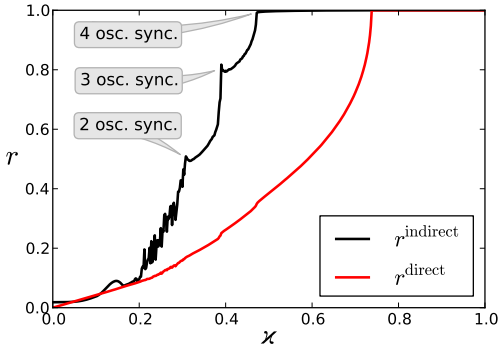

FIG. 3. (Color online) Transition to phase synchronization for the hub motif [Fig. 1]. From the plot the onset of RS is clearly visible. The three annotations indicate synchronization between two, three and four peripheral oscillators, respectively.

are shown. This figure is discussed in more detail later in the article.

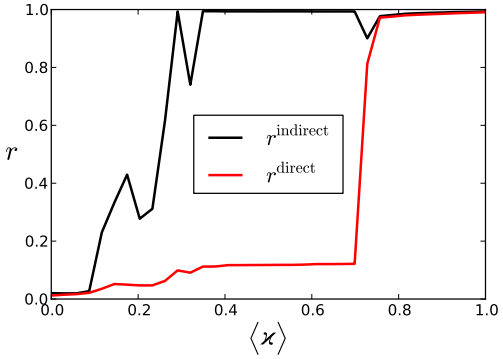

FIG. 4. (Color online) Transition to phase synchronization for the hub motif for experimentally obtained data. The regime of RS is clearly visible.

Fig. 4 shows the same plot for experimentally generated data. The data have been obtained by a set of experiments on the implemented network of Stuart-Landau oscillator circuits performed with respect to different values of the coupling $\varkappa$, starting from $\varkappa = 1.0$ and decreasing this parameter. The coupling strength is decreased by small steps and for each value of it, the state variable x_n for each circuit has been acquired with a National Instruments USB6255 acquisition board with the sampling frequency $f_s = 300kHz$. The phases of the oscillators have been then calculated by applying the Hilbert transform on the obtained time series and the two parameters r^{indirect} and r^{direct} have been calculated. The result, shown in Fig. 4, confirms the existence of RS in real systems. It should be noted that the coupling strength is implemented in the circuit through five different components, which makes it quite difficult to obtain exactly the same value for it, taking also into account the tol-

erances in the whole network circuit. For this reason, in Fig. 4 the average value $\langle \varkappa \rangle$ of this parameter is reported. The scenario observed is qualitatively similar to that obtained with numerical data, and the two transitions occur at slightly different values of the parameter. It is clearly visible that there exists a quite large domain of the coupling parameter, where we have RS while the hub remains with its own dynamics.

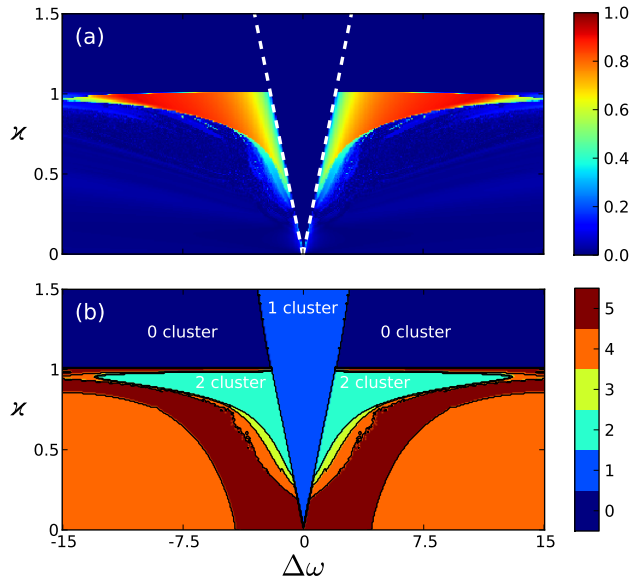

FIG. 5. (Color online) Fig (a) shows Δr in dependence on $\Delta\omega$ and $\varkappa$, which can assume values between 0 and 1, whereby values close to 1 indicate RS (see text). The dotted line shows the analytically derived border of the Arnold tongue. The red areas to the left and right of the Arnold tongue are regimes in which RS occurs. Fig (b) depicts the number of LEs equal to zero in dependence on $\Delta\omega$ and $\varkappa$. The 2-cluster state corresponds to the RS regime.

As a second analysis tool we are computing the Lyapunov spectrum (LS). Any non-trivial attractor (limit cycle, chaotic) of continuous dynamical systems has one Lyapunov exponent (LE) equal to zero, corresponding to the free phase of that system. Any perturbation in the direction of the system's flow will remain constant over time. In the case of an ensemble of uncoupled systems with a limit cycle or chaotic attractor, there will be as many zero LEs as there are systems included. As one couples those systems, PS will manifest itself by one or more (depending on the number of sub-systems forming the synchronized cluster) LEs becoming strictly negative due to the attractive force between the former free phases of the oscillators [22]. Hence, the number of LEs equal to zero can be used as an indirect measure for the number of phase synchronized clusters.

In order to examine this phenomenon in more detail, we also studied the clustering in dependence on the hub's frequency. In Fig. 5(a) we plot $\Delta r := |r^{\text{direct}} - r^{\text{indirect}}|$ in dependence on the global coupling strength $\varkappa$ and the frequency mismatch $\Delta\omega$ of the hub with respect to the mean frequency of the peripheral nodes: $\Delta\omega := \omega_1 - \langle\omega_n\rangle_{n=2}^{N}$. In the case of RS r^{indirect} will be close to 1, while r^{direct} will be rather low, say less than 0.5, so Δr will be large here. If we are either in a regime where we have no synchronization or full synchronization r^{direct} and r^{indirect} will be about equal (either around 0 or around 1) and thus Δr will be low.

Fig. 5(b) shows the number of LEs equal to zero for the same parameters $\Delta\omega$ and $\varkappa$. As already mentioned, this is an indirect measure for the number of synchronized clusters.

The red area in Fig. 5(a) corresponds to the regime where RS exists. We find the same shape in Fig. 5(b) with a value of 2, thus showing that we have two synchronized clusters here. Both measures are in very good agreement with each other. For coupling strengths $\varkappa > 1$ and outside the Arnold tongue we have oscillation death, which manifests in the Lyapunov spectrum by all LEs becoming negative, since the system has only one global stable fixpoint. In both figures we clearly see the classical V-shaped Arnold tongue of the globally synchronized state, i.e. a regime of one cluster PS.

For system (1), the Arnold tongue $\mathcal{A}$ can be computed analytically:

$$\mathcal{A} = \{(\varkappa, \{\omega_n\}_{n=1}^{N}) \mid \varkappa > \max_n |\Omega - \omega_n|\},$$

where Ω is the frequency inside the Arnold tongue, given by

$$\Omega = \frac{1}{2}\left(\omega_1 + \frac{1}{N-1}\sum_{n=2}^{N}\omega_n\right).$$

In Fig. 5(a) the analytically computed border of $\mathcal{A}$ is shown with dotted lines and agree very well with the border observed from the numerically integrated data.

In the following we discuss the basic mechanism of RS and give an explanation for the necessary conditions for RS to occur robustly. We first describe the mechanism verbally and give a mathematical derivation afterwards.

IV. MECHANISM UNDERLYING REMOTE SYNCHRONIZATION

Since we are interested in the mechanism of how two indirectly connected oscillators become synchronized, it is sufficient to focus on three nodes only: two peripheral nodes, to which we will refer to as node 2 and node 3 (in correspondence with our initially made numbering), connected indirectly via the hub (node 1). In order for node 2 and node 3 to mutually synchronize, actions of node 2 need to be transmitted to node 3 and vise versa. It means that the dynamics of node 1 have to be such that they leave the transmitted actions of node 2 and node 3 possibly unaltered. Thus, two conditions have to be fulfilled for RS to occur. Firstly, the average time scale

of the attractor of node 1 should be sufficiently different from the ones of the attractors of node 2 and node 3 in order to not to synchronize with them. Furthermore, node 2 and node 3 must not be too different such that they are able to synchronize through a weak interaction. Secondly, perturbations of node 1 must not decay too fast in order to get transmitted via node 1.

The decay of perturbations of the Stuart-Landau oscillator is controlled by the parameter α in Eq. (1). The larger α the faster a deviation from the limit cycle will "fall back" onto that. For $\alpha \to \infty$ any deviation of the amplitude will decay immediately. Thus, we expect the RS regime disappears for $\alpha \to \infty$. In this case, after a change into polar coordinates and omitting the amplitude, Eq. (1) can be transformed into a network of coupled Kuramoto phase oscillators [7, 23]:

$$\dot{\varphi}_n = \omega_n \ + \ \frac{\varkappa}{d_n^{\text{in}}} \sum_{m=1}^{N} g_{nm} \sin(\varphi_m - \varphi_n), \qquad (4)$$

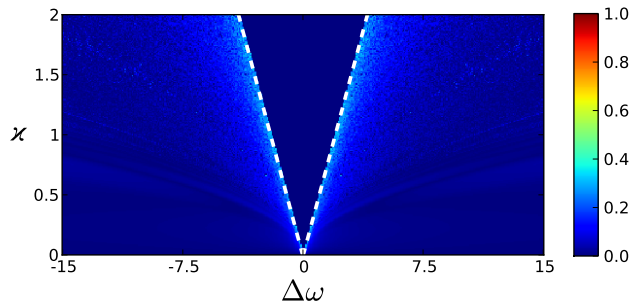

FIG. 6. (Color online) $\Delta r(\Delta\omega, \varkappa)$ for the hub motif of Kuramoto phase oscillators [Eq. (4)] is shown. By comparing with Fig. 5(a) it can be observed that there is no RS regime, here.

We applied the analysis described in Sec. III to this network of phase oscillators using the same setup and parameters as in the Stuart-Landau case described in Sec. II. Fig. 6 shows $\Delta r(\Delta\omega, \varkappa)$ for this system. By comparing Fig. 6 with Fig. 5(a) the absence of the RS regime for the phase oscillators is clearly visible (absence of the red areas to left and right of the Arnold tongue which indicate RS). We have also checked that by computing Δr for different increasing values of α. In this case the disappearance of the RS can be tracked. Thus, our previously made assumption is correct, that the ability of indirectly coupled oscillators to synchronize remotely depends on a certain flexibility or memory of the amplitude of the transmitting system. Or even more crucial, it depends on the existence of a free amplitude at all. We show in fact that when amplitude perturbation is not possible, as for instance in coupled Kuramoto phase oscillators, for which a fixed not perturbable amplitude is assumed indirectly, remote synchronization does not appear!

Interesting is the dependence on the hub's frequency of the RS state, which can not be explained with the above argumentation, alone. In the following we derive some analytic description, which qualitatively account for that.

We come back to the situation of three coupled Stuart-Landau oscillators as discussed in the beginning of this section. We linearize the hub oscillator around its limit cycle and leave the other two nodes untouched. We get the following equations:

$$\dot{u}_{\text{h}} = (-2\alpha + i\omega_{\text{h}})u_{\text{h}} \ + \ \tfrac{1}{2}\varkappa(u_1 + u_2 - 2u_{\text{h}}) \qquad (5)$$

$$\dot{u}_{1,2} = (\alpha + i\omega_{1,2} - |u_{1,2}|^2)u_{1,2} \ + \ \varkappa(u_{\text{h}} - u_{1,2}). \qquad (6)$$

These equations describe two Stuart-Landau oscillators [Eq. (6)] coupled through a linear filter whose dynamics is described by the Eq. (5). Applying the Laplace transform we can write the transfer function for this filter:

$$H_{\text{h}}(\omega) \ = \ \frac{\varkappa}{i\omega + 2\alpha + \varkappa - i\omega_{\text{h}}}. \qquad (7)$$

Using this, the hub can be replaced by an effective coupling coefficient, which is just a number derived from Eq. (7). Thus, we can write

$$\dot{u}_{1,2} = (\alpha + i\omega_{1,2} - \varkappa - |u_{1,2}|^2)u_{1,2} \ + \ \varkappa H_{\text{h}}(\omega_{2,1})u_{2,1}. \quad (8)$$

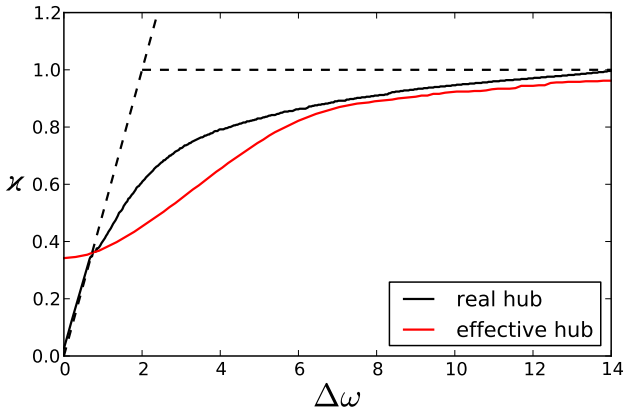

FIG. 7. (Color online) Comparison of the transition lines to RS between a system of three nodes (real hub), described by Eq. (1) with $N = 3$, and the linear approximation, described by Eqs. (8) and (7). The frequencies of node one and two are 0.975 and 1.025, respectively. The frequency of the hub has been changed from 1 to 15 (corresponds to $1 + \Delta\omega$). The dotted lines mark the regions of the Arnold tongue and of oscillation death, respectively, and are inserted to help the reader by comparing with Fig. 5

From this perspective we are able to explain two main properties: Firstly, obviously since $\lim_{\alpha\to\infty} H_{\text{h}} = 0$ the effective coupling strength between the two peripheral oscillators drops to zero and they are effectively uncoupled and, thus, unable to synchronize. This confirms our previous discussion of the mechanism as well as the numerically made analysis with Kuramoto phase oscillators. Secondly, by inspection of Eq. (7) the dependence of the

coupling strength on the frequency of the hub is clear. The faster the hub oscillates the lower the effective coupling strength will be. Fig. 7 shows the transition curve to RS in the $(\Delta\omega, \varkappa)$-plane for the discussed system of three oscillators in comparison with the system of two effectively coupled oscillators as described by Eqs. (8) and (7). The simplified system can qualitatively describe the made observations and even agrees quantitatively for low and high values of the frequency mismatch $\Delta\omega$ adequately.

V. REMOTE SYNCHRONIZATION IN COMPLEX NETWORKS

In this section we want to give a short outlook on RS in complex networks. We will not discuss the phenomenon in detail in this context, as it needs a lot more preparation and advanced statistical methods for a detailed analys, since far more complex synchronization scenario are possible. However, one is able to find RS in more complex and asymmetric networks as well. For our demonstration we generated a network consisting of 100 nodes using the Barabási-Albert algorithm [17].

Fig. 8 illustrates the scenario of remote synchronization in this exemplary complex network. The parameters used for this simulation have been: $\varkappa = 0.21$ and $\alpha = 0.2$. The frequencies of all nodes have been drawn randomly from a uniform distribution on small interval of size 0.1 centered at 3.5 for the hubs and 1.0 for the remaining nodes. The plot shows overlaid the actual (physical) network topology as it has been generated. The thick transparent lines depict synchronized nodes. Two nodes n and m have been declared phase synchronized if their PS index is $r_{nm} > 0.95$. The different coloring have been chosen to guide the readers eye. Gray coloring indicates synchronization between peripheral (non-hub) nodes while red color shows synchronization between two hub-nodes.

In this chosen situation many remotely synchronized clusters can be spotted, visual by many gray lines spanning across the network. Some of those clusters even spread across long distances with several hub nodes lying in between which are not synchronized with the former. Further the hub nodes connecting the remotely synchronized clusters are synchronized itself into a cluster. This is especially interesting since the topology one would infer from analyzing the synchronization state of the network does not reflect even closely the physical connectivity of the nodes.

VI. HIDDEN INFORMATION TRANSFER

Finally we want to stress another important point. From our study we conclude that in the analysis of complex heterogeneous systems the choice of an appropriate correlation or information measure becomes more important. We demonstrate this with an example. Analogously to Eq. (3) we introduce another measure

$$\rho_{nm} = \left| \langle e^{i[\theta_n(t) - \theta_m(t)]} \rangle_t \right|, \tag{9}$$

where $\theta(t) = \arctan[\mathcal{H}\ddot{\varphi}(t)/\ddot{\varphi}(t)]$ and $\mathcal{H}$ is the Hilbert transform operator (see appendix in [18] for details). We use the second derivative of φ in order to eliminate the bias. The measure ρ is an index for PS between the modulations of the instantaneous frequencies $\dot{\varphi}$, which are visible in Fig. 2(a) and (b). From visual inspection of those figures one sees that in the case of remote synchronization these modulations of $\dot{\varphi}$ are in synchrony among all nodes. Fig 9 shows for the same data which

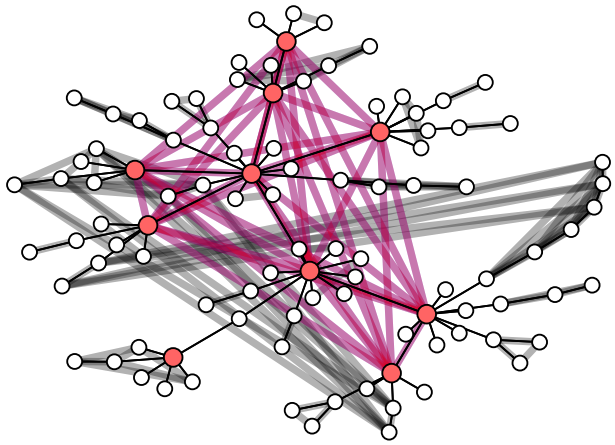

FIG. 8. (Color online) Graphical representation of remote synchronization scenario in a scale-free network consisting of 100 nodes. Nodes with five or more links have been declared as hub and are colored red. The hubs have a mean frequency of 3 while the remaining nodes have a mean frequency of 1. For each pair of nodes n and m a thick transparent line has been drawn if $r_{nm} > 0.95$, i.e if both nodes can be assumed to be phase synchronized with respect to the PS order parameter r. Gray lines have been drawn between peripheral nodes and red lines between hubs. See text for more details.

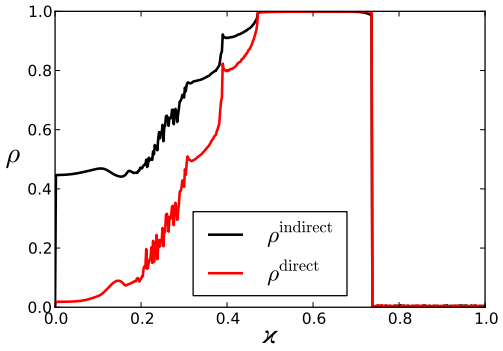

FIG. 9. (Color online) Transition of phase synchronization for the modulation of the instantaneous frequency of the nodes.

had been used to create Fig 3 the measures ρ^{direct} and ρ^{indirect} which are analogously computed to r^{direct} and r^{indirect} with r replaced by ρ. From the resulting graph one clearly sees that the phase modulations of all the oscillators in the network synchronize completely already at the first transition for $\varkappa \approx 0.47$. At $\varkappa \approx 0.74$ ρ drops to zero which is due to the disappearance of the phase modulations (oscillation death due to a Hopf bifurcation, see [24]). With the measure ρ we are able to track the increase of the information transmission within the network. Other nonlinear phase space based measures (such as described in [25]) are also able to track this transition. In more complex network this or similar method could be used to track the path through which certain remotely synchronized oscillators communicate. This is of special importance in particular related to the issue of inferring the network topologies from measured time series. Our example demonstrates that by using simple PS measures (as for instance r) the network's physical connectivity is obfuscated, but choosing other measures or–even better– combinations of different measures improved statements about the true connectivity of networks can be made.

VII. CONCLUSIONS

Our findings shed some new light on the issue of functional versus structural topology in networks of interacting dynamical systems, which is of high importance especially in the field of neuroscience. We have shown that the measured topology via a "naïve" phase synchronization measure gives a wrong picture of the underlying network structure and explained this by a mechanism which we call remote synchronization (RS). Nodes can "speak" with each other through a transmitting nodes without synchronizing with this one, given that the transmitter has a sufficiently different frequency.

We verified that RS also occurs in real experiments, by designing a network of five coupled oscillators showing the regime of RS for coupling strength values which are intermediate between the case of no synchronization and that of PS of the whole network. Therefore, not purely phase oscillators may reveal phenomena that can be experimentally observed and that purely phase models are not able to explain.

We expect that the same phenomenon of RS occurs in more complex topologies as confirmed by some preliminary results including those obtained on scale-free networks as discussed above. RS can be also important with anharmonic or chaotic oscillators, where more complicated dynamics are possible.

RS might also find applications in several fields, such as neuroscience, here in understanding information transmission inside the brain or help designing new more efficient artificial neural networks as described in [6]. Another application might be in climate research, in particular in understanding teleconnections (i.e long-range connections) such as between the Indian Monsoon and El Niño/Southern Oscillation [10, 11, 26].

ACKNOWLEDGEMENTS

This work was supported by DAAD/Ateneo Italo-Tedesco under the VIGONI Project and ECONS (WGL).

Appendix A: Circuit

An assembly of coupled electronic circuits was used to test remote synchronization in real physical systems. In this Appendix, the electronic oscillator used and the coupling circuitry between the oscillators are briefly described.

The circuit that was built is governed by a rescaled version of Eqs. (2), i.e. $\frac{d}{dt} \to \tau \frac{d}{dt}$, where τ is a time scaling factor ($\tau = 10^{-5}s$ in our circuit). The other circuit parameters were set to the values discussed in Section II. Figure 10 shows a schematic of the circuit. The values of the circuit components have been chosen in order to match Eqs. (2). In particular, the relationships between the parameters α and ω and the component values are given by:

$$\begin{aligned} \alpha &= \frac{R_6}{R_1} - 1 = \frac{R_{13}}{R_{10}} - 1 \\ \omega &= \frac{R_6}{R_4} = \frac{R_{13}}{R_{11}} \end{aligned} \tag{A1}$$

Eqs. (A1) have been used to set the component values for the hub circuit and for the peripheral nodes. The component values listed in the caption of Fig. 10 refer to a peripheral node. The hub components differ from that of a peripheral node for the following resistors: $R_3 = 667\Omega$, $R_4 = 400\Omega$, $R_{11} = 1.6k\Omega$, $R_{12} = 727\Omega$. Resistors with 1% tolerances and capacitors with 5% tolerances have been used.

The experimental coupled oscillator setup consisted of five circuits arranged in a star-like network. The coupling terms $\varkappa(x_j - x_i)$ and $\varkappa(y_j - y_i)$ are produced by adding the x (respectively y) signals and multiplying them for a tunable gain factor through an operation amplifier in algebraic adder configuration. The tuning of the coupling coefficient is realized by using as feedback resistor a potentiometer. The coupling terms are then added into the equations of the electronic oscillator through the operational amplifier adders U1 [term $\varkappa(x_j - x_i)$] and U2 [term $\varkappa(y_j - y_i)$].

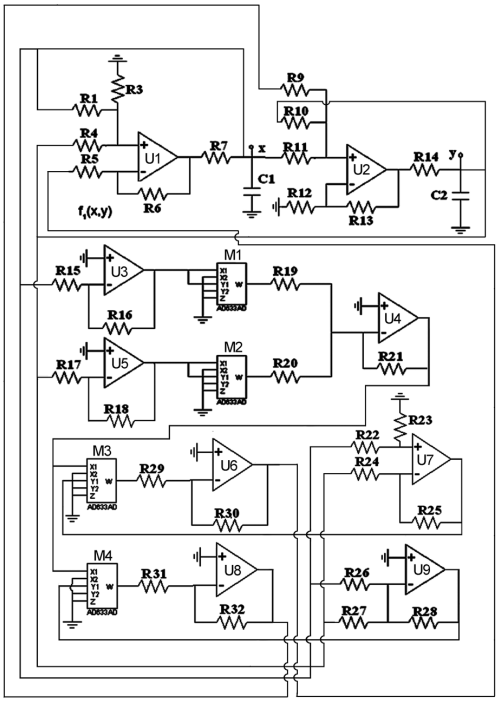

FIG. 10. Schematic of the circuit described by Eqs. (2) (rescaled in time with τ). The component values are: $R_1 = 500\Omega$, $R_3 = R_4 = R_5 = R_6 = 1k\Omega$, $R_6 = 100\Omega$, $R_8 = R_9 = 4k\Omega$, $R_{10} = 2k\Omega$, $R_{11} = 4k\Omega$, $R_{12} = 1k\Omega$, $R_{13} = 4k\Omega$, $R_{14} = 100\Omega$, $R_{15} = 1k\Omega$, $R_{16} = 7.2k\Omega$, $R_{17} = 1k\Omega$, $R_{18} = 7.2k\Omega$, $R_{19} = R_{20} = R_{21} = R_{22} = 1k\Omega$, $R_{23} = R_{24} = 2k\Omega$, $R_{25} = 1k\Omega$, $R_{26} = 2k\Omega$, $R_{27} = R_{28} = R_{29} = R_{30} = R_{31} = R_{32} = 1k\Omega$, $C_1 = C_2 = 100nF$. The operational amplifiers $U1, \ldots, U9$ are all type TL084. The analog multipliers $M1, \ldots, M4$ are all type AD633. Power supply is $\pm 9V$.

[1] S. Boccaletti, V. Latorab, Y. Morenod, M. Chavezf, D.-U. Hwanga, *Complex networks: Structure and dynamics*, Phys. Rep., 424, 175308, 2006.

[2] A. Arenas, A. Diaz-Guilera, J. Kurths, Y. Moreno, C. Zhou, *Synchronization in complex networks*, Phys. Rep., 469, 93, 2008

[3] G. V. Osipov, J. Kurths, C. Zhou, *Synchronization in Oscillatory Networks*, Springer-Verlag Berlin, 2007.

[4] S. Gil, A. S. Mikhailov, *Networks on the edge of chaos: Global feedback control of turbulence in oscillator networks*, Phys. Rev. E, 79, 026219, 2009.

[5] E. M. Izhikevich, *Dynamical Systems in Neuroscience: The Geometry of Excitability and Bursting*, MIT Press, 2006.

[6] F. C. Hoppensteadt, E. M. Izhikevich, *Oscillatory Neurocomputers with Dynamic Connectivity*, Phys. Rev. Lett., 82, 14, 1999.

[7] Y. Kuramoto, *Chemical Oscillations, Waves, and Turbulence*, Springer-Verlag Berlin Heidelberg, 1984.

[8] E. Ullner, A. Koseska, J. Kurths, E. Volkov, H. Kantz, J. Garca-Ojalvo, *Multistability of synthetic genetic networks with repressive cell-to-cell communication*, Phys. Rev. E, 78, 031904, 2008.

[9] J.F. Donges, Y. Zou, N. Marwan, and J. Kurths, *Complex networks in climate dynamics*, Eur. Phys. J. Special Topics, 174, 157179, 2009.

[10] J. F. Donges, Y. Zou, N. Marwan and J. Kurths, *The backbone of the climate network*, EPL, 87, 48007, 2009.

[11] D. Maraun, J. Kurths, *Epochs of phase coherence between El Niño/Southern Oscillation and Indian monsoon*, Geophys. Res. Lett., 32, L15709, 2005.

[12] D. He, L. Stone, *Spatio-temporal synchronization of recurrent epidemics*, Proc. R. Soc. Lond. B 270, 15191526, 2003.

[13] S. Gil, D. H. Zanette, *Coevolution of agents and networks: opinion spreading and community disconnection*, Phys. Lett. A 356, 8995, 2006.

[14] A. Buscarino, C. Camerano, L. Fortuna, M. Frasca, *Chaotic Mimic Robots*, Phil. Trans. R. Soc. A, 368, 2179-2187, 2010.

[15] A. Buscarino, L. Fortuna, M. Frasca, *Separation and Synchronization of Chaotic Signals by Optimization*, Phys. Rev. E, 75, 016215, 2007.

[16] K. Konishi, H. Kokame, *Synchronization of pulse-coupled oscillators with a refractory period and frequency distribution for a wireless sensor network*, Chaos, 18 (3), 033132, 2008.

[17] R. Albert, A.-L. Barabási, *Statistical mechanics of complex networks* Rev. mod. Phy., 74, 2002.

[18] A. Pikovsky, M. Rosenblum, J. Kurths, *Synchronization - A universal concept in nonlinear science*, Cambridge University Press, 2001.

[19] L. Fortuna, M. Frasca, M.G. Xibilia, *Chua's Circuit Implementations: Yesterday, Today and Tomorrow*, World Scientific Series on Nonlinear Science, Series A - Vol. 65, 2009.

[20] E. J. Ngamga, A. Buscarino, M. Frasca, L. Fortuna, A. Prasad, J. Kurths, *Recurrence analysis of strange nonchaotic dynamics in driven excitable systems*, Chaos, 18 (1), 013128-1-8, 2008.

[21] A. Buscarino, L. Fortuna, M. Frasca, *Robust synchronization of hyperchaotic circuits*, Physica D, 238, 1917-1922, 2009.

[22] M. Rosenblum, A. Pikovsky, J. Kurths, *Phase Synchronization of Chaotic Oscillators*, Phys. Rev. Lett. E, 76 (11), 1804-1807, 1996.

[23] J. A. Acebrón, L. L. Bonilla, C. J. Prez Vicente, F. Ritort, R. Spigler, *The Kuramoto model: A simple paradigm for synchronization phenomena*, Rev. Mod. Phys., 77, 137185, 2005.

[24] D.G. Aronson, G.B. Ermentrout, N. Kopell, *Amplitude response of coupled oscillators*, Physica D, 41, 403-449, 1990.

[25] T. Pereira, M. S. Baptista, J. Kurths, *General framework for phase synchronization through localized sets*, Phys. Rev. E 75, 026216, 2007.

[26] I. I. Mokhov, D. A. Smirnov, P. I. Nakonechny, S. S. Kozlenko, E. P. Seleznev, J. Kurths, *Alternating mutual influence of El-Niño/Southern Oscillation and Indian monsoon*, Geophys. Res. Lett., 38, L00F04, 2011.